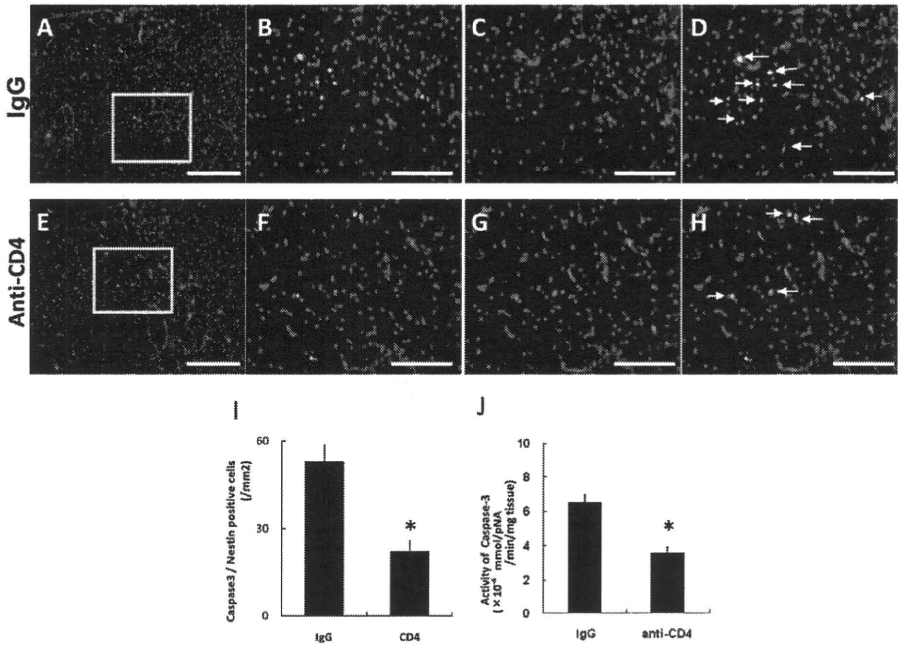

Fig. 6. Depletion of CD4-positive T lymphocytes reduces neural stem/progenitor cells apoptosis. Immunohistochemical analysis for nestin (red)-/caspase-3 (green)-positive cells was performed in sections from the mice treated with anti-CD4 or control IgG on day 3 after stroke (A,E, lower magnification; B–D,F–H, higher magnification; A,D,E,H, merged image; B,F, caspase-3; C,G, nestin). In **A–H**, nuclei were counterstained with DAPI [blue]. **I:** Quantitative analysis revealed that removal CD4-positive T cells decreased the number of nestin-/caspase-3-positive cells at the border of infarction compared with the control. **J:** The level of caspase-3 activity in the infarcted tissue was significantly decreased in the mice treated with anti-CD4 compared with control on day 7 after stroke. In I,J, n = 3 for each experimental group. *$P < 0.05$ vs. control IgG group. Scale bars = 500 μm in A,E; 200 μm in B–D,F–H.

panels, lower magnification; lower panels, higher magnification). Quantitative analysis revealed a significant increase in the number of NeuN/BrdU double-positive cells in mice treated with anti-CD4 antibody compared with animals receiving control IgG (Fig. 7B).

Finally, functional recovery was evaluated in poststroke mice treated with anti-CD4 or anti-CD8 antibody by behavioral testing. Locomotor activity was measured by using an open field apparatus at 28 days after stroke. Groups treated with control IgG and anti-CD8 antibody showed greater exploratory activity than the other groups. The activity of the mice treated with anti-CD4 antibody was maintained at the same level as in sham-operated mice (n = 8, 28 days after sham operation with no treatment; Fig. 7C). This impression was supported by a group (4) × period (2: light vs. dark) ANOVA, which indicated significant main effects of group [$F(3, 35) = 3.86$, $P < 0.05$] and period [$F(1, 35) = 28.66$, $P < 0.00001$]. The interaction of group × period was not significant [$F(3, 35) = 1.05$, $P = 0.381$]. Subsequent Fisher's LSD tests revealed that locomotor activity of the mice treated with anti-CD4 antibody was significantly suppressed vs. control IgG- and anti-CD8 antibody-treated groups ($P < 0.01$ and $P < 0.05$, respectively). Differences in locomotor activity between mice treated with anti-CD4 antibody and sham-operated controls were not significant. The absence of a difference between the latter two groups suggested improvement of neural/neuronal function in animals treated with anti-CD4 antibody.

Impaired Endogenous Neurogenesis on Depletion of Regulatory T Cells

Because the population of CD4-positive T lymphocytes has included immunosuppressive regulatory T (Treg) cells (Liesz et al., 2009), depletion of CD4-positive cells might affect on the Treg function. To investigate the role of Treg cells in the endogenous neurogenesis after stroke, CD25-positive T cells were depleted from CB-17 mice by administration of antibody to CD25 one day before and 3 days after stroke (Fig. 8A). As a result, the number of nestin/BrdU double-positive cells at the border of infarction was significantly reduced in mice treated with CD25 antibody compared with IgG-treated controls on day 7 after stroke (Fig. 8B). On day 28 after stroke, neuronal function was impaired to a greater extent in poststroke animals treated with anti-CD25 antibody com-

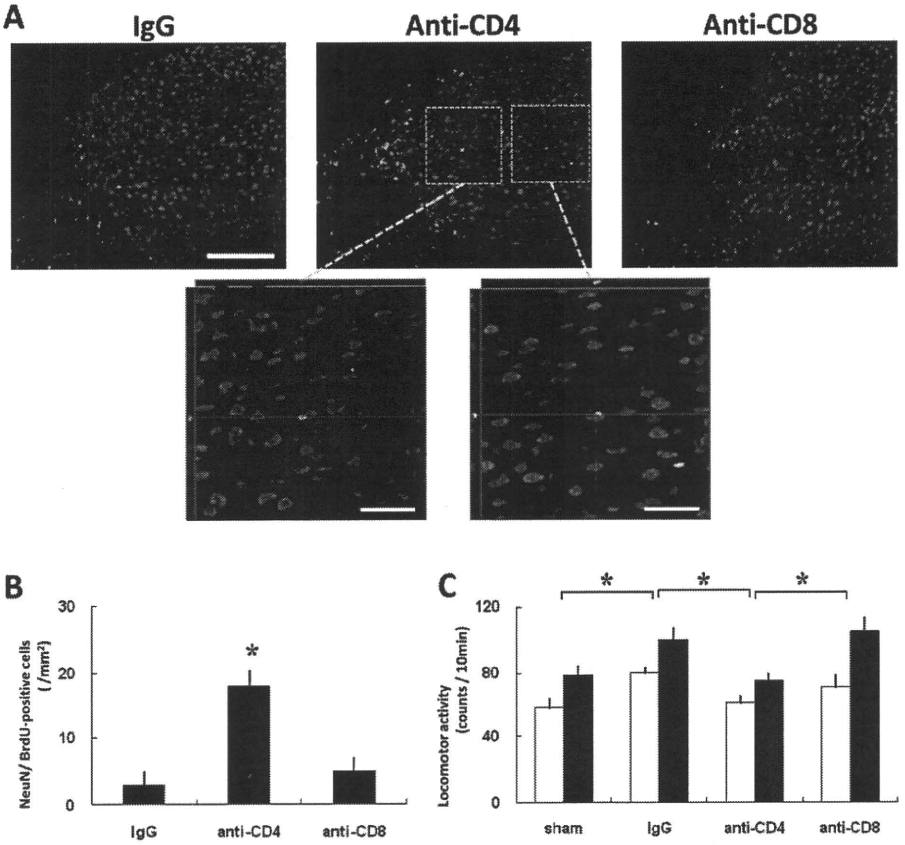

Fig. 7. Depletion of CD4-positive T lymphocytes enhances endogenous neurogenesis and functional recovery in vivo. **A:** Some NeuN (red)/BrdU (green) double-positive cells were observed at the border of infarction in anti-CD4-treated mice on day 28 after stroke. In contrast, fewer double-positive cells were observed in anti-CD8-treated mice or animals treated with control IgG (upper panels, lower magnification; lower panels, higher magnification). Higher magnification panels show the x-z and y-z cross-sections produced by orthogonal reconstructions from z-series with a confocal laser scanning microscope. **B:** Quantitative analysis confirmed a significant increase in number of NeuN-/BrdU-positive cells in anti-CD4-treated mice compared with the controls (n = 3 for each experimental group; studies were done 28 days poststroke in each case). **C:** Improvement in behavioral function, based on the open field task, was observed in CB-17 mice treated with anti-CD4 antibody (n = 14) compared with sham-operated (n = 8), control IgG (n = 9), and anti-CD8 antibody (n = 8) at 28 days after stroke (open bars, light period; solid bars, dark period). $^*P < 0.05$. Scale bars = 500 μm (lower magnification); 50 μm (higher magnification).

pared with those receiving control IgG (Fig. 8C). This impression was supported by a group (2) × period (2: light vs. dark) ANOVA. The main effect of group was not significant ($F < 1$), but the interaction of group × period was significant [$F(1, 13) = 18.37$, $P < 0.01$]. The main effect of period [$F(1, 13) = 4.55$, $P = 0.053$] was marginally significant. Subsequent Fisher's LSD tests revealed that locomotor activity during the light period for mice treated with anti-CD25 antibody was significantly increased vs. the control IgG-treated group ($P < 0.01$), the latter showing hyperactivity compared with sham-operated mice. The difference between the two groups suggested worsening of neural/neuronal function in CB-17 animals treated with anti-CD25 antibody. Morphologic analysis showed the enhanced injury to poststroke brain in animals receiving anti-CD25 antibody, based on evaluation of hemisphere volume (Fig. 8D).

DISCUSSION

Our findings demonstrate a key role of T lymphocytes in the regulation of neurogenesis after brain injury, thereby delineating a contribution of the immune system to the survival of neural stem/progenitor cells in vivo. Recent publications have proposed such immune cells as a modulator of poststroke inflammatory response, in which CD4-positive T cells enhance the brain injury after transient cerebral ischemia (Yilmaz et al., 2006;

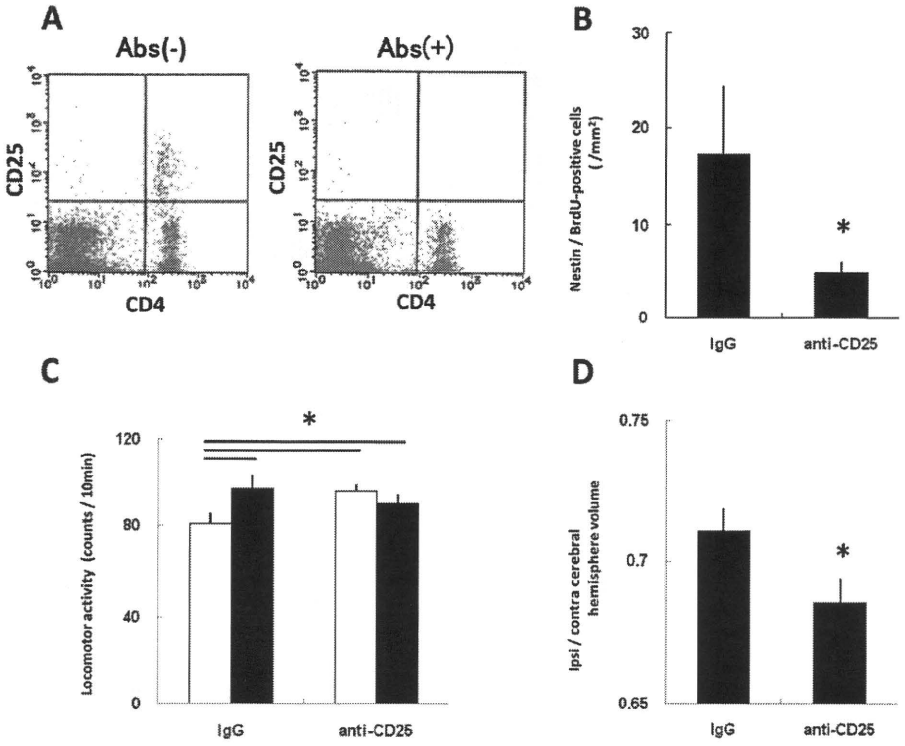

Fig. 8. Depletion of regulatory T lymphocytes impairs endogenous neurogenesis. **A:** Antibody-induced depletion of CD25 T cells was confirmed by FACS. **B:** Quantitative analysis on day 7 after stroke revealed that depletion of CD25-positive T cells significantly reduced the number of nestin/BrdU-positive cells at the border of infarction compared with IgG-treated controls. **C:** Impaired behavior, based on the open field task, was observed in CB-17 mice treated with anti-CD25 antibody (n = 6) compared with those receiving control IgG (n = 9) at 28 days after stroke (open bars, light period; solid bars, dark period). **D:** Morphological study based on the brain volume confirmed the poststroke damage enhanced by treatment with anti-CD25 antibody compared with control (n = 6 each). $*P < 0.05$ vs. control IgG group.

Hurn et al., 2007), whereas CD25-positive T cells, which include CD4-positive regulatory T cells (Treg cells), are cerebroprotective targeting multiple inflammatory pathways (Liesz et al., 2009). Although these reports have focused on their contribution to brain injury, our current results may suggest for the first time that immune cells could contribute to neural repair at the level of neural stem/progenitor cells.

The neural stem/progenitor cells are known to be present throughout the adult brain and to proliferate after ischemic insult (Itoh et al., 2005). We also have demonstrated that endogenous neural stem/progenitors with the potential to differentiate into neurons can develop within the poststroke cerebral cortex (Nakagomi et al., 2009). However, for immunocompetent animals, it appeared that T lymphocytes infiltrate the ischemic cerebral cortex, thereby exerting a negative effect, such as apoptotic cell death, on nestin-positive cells. This suggests the presence of cytotoxicity by T lymphocyte, either directly or indirectly, on the neural stem/progenitor cells developed within the poststroke cerebral cortex.

In this context, a direct effect of T lymphocytes on neurons has been reported. Infiltration of CD4-positive T lymphocytes, which include subsets of cytotoxic T cells (Mukherji et al., 1989, 1990), into the brain contributes to neurodegeneration in a mouse model of Parkinson's disease (Brochard et al., 2009). Brochard et al. showed that removal of CD4- but not CD8-positive T cells in mice greatly reduced MPTP-induced nigrostriatal cell death and that the deleterious activity of infiltrating CD4-positive T cells involved the Fas/FasL pathway. In vitro experiments have also demonstrated an apparently high and selective vulnerability of human neurons to T cells and provide support for a deleterious effect of activated T cells consequent to their accumulation in the CNS.

As for Fas system effects on neural stem cells, recent reports have shown that Fas activates cultured adult neural stem cells when it is stimulated by pretrimerized soluble FasL, suggesting that Fas does not trigger apoptosis (Corsini et al., 2009). However, more recently, it has been demonstrated that membrane-bound Fas ligand only is essential for Fas-induced apoptosis,

whereas soluble FasL induces nonapoptotic signals on Fas-expressed cells (O'Reilly et al., 2009), and that Fas agonists that bind the same Fas receptor initiate mechanistically distinct pathways resulting in differential cytotoxicity (Morgan et al., 2009). Our current results showed the expression of Fas antigen on nestin-positive cells, which undergoes apoptosis through a Fas-mediated pathway in vivo. This suggests that a protective effect found in immunodeficient mice may be related, at least in part, to the direct action of CD4-positive T lymphocytes infiltrating poststroke cerebral cortex employing a Fas-mediated cell death pathway. Similarly to our current results, the causative role of CD4-positive T lymphocytes has been reported in certain models/settings of multiple sclerosis (Delgado and Sheremata, 2006).

In view of the cytotoxic effects of T lymphocytes on neural stem/progenitors, depletion of CD4-positive cells solely might not sufficiently inhibit their apoptosis, because a subtype of CD4-positive T cells, regulatory T (Treg) cells (CD4/CD25/FoxP3-positive), is known to suppress the function of activated CD4-positive T cells (Liesz et al., 2009). Depletion of CD25-positive T cells is known to enhance brain damage through activation of the immune response. Our data suggest that CD25-positive T cells also may contribute to the regulation of neurogenesis as well as the progression of neuronal injury after stroke.

In another context, T lymphocytes are proposed as a modulator of poststroke inflammatory response, in which activated astrocytes and microglia have been shown to exert both positive and negative effects on tissue repair after stroke (Chen et al., 1993; Van Beek et al., 2000; Ito et al., 2001). Several studies have shown a beneficial effect of activated microglia on CNS repair after brain injury (Butovsky et al., 2006; Jakubs et al., 2008), secreting multiple cytokines to modulate CNS inflammation (Nishi et al., 2005; Rasley et al., 2006; Clausen et al., 2008; Lambertsen et al., 2009). In this report, however, we could not find significant differences in cytokine levels or in the number of Iba-1-positive cells within the infarcted area between immunodeficient and immunocompetent mice, although the immunodeficiency has been reported to reduce the poststroke inflammation. Insofar as the number of microglia has been reported originally to be increased in the brain of immunodeficient mice (Lorke et al., 2008), it is possible that the difference in levels of cytokines expressed mainly in microglia could not be detected in the current study. In addition to such glial cells, the contribution of other immune cells, including B lymphocytes and other subset of T lymphocytes, to the neural repair after stroke should be examined more in detail in the future.

We propose that lymphocytes within the CNS serve as negative regulators in the survival of neural stem/progenitor cells. The positive impact of such a mechanism under homeostatic conditions would be to prevent unnecessary generation/expansion of immature neural cells. However, the adverse implications of such negative control are obvious in settings of neuronal loss, such as stroke. This program balances mechanisms involving eventual neural regeneration vs. those favoring death of injured neural cells. The present study suggests that neural repair after stroke may be accelerated by a transient modulation of the immune system, providing a novel therapeutic approach.

ACKNOWLEDGMENTS

We thank Y. Okinaka, Y. Tanaka, and Y. Kasahara for their technical assistance.

REFERENCES

Arvidsson A, Collin T, Kirik D, Kokaia Z, Lindvall O. 2002. Neuronal replacement from endogenous precursors in the adult brain after stroke. Nat Med 8:963–970.

Brochard V, Combadiere B, Prigent A, Laouar Y, Perrin A, Beray-Berthat V, Bonduelle O, Alvarez-Fischer D, Callebert J, Launay JM, Duyckaerts C, Flavell RA, Hirsch EC, Hunot S. 2009. Infiltration of $CD4^+$ lymphocytes into the brain contributes to neurodegeneration in a mouse model of Parkinson disease. J Clin Invest 119:182–192.

Brown KM, Donohue DE, D'Alessandro G, Ascoli GA. 2005. A cross-platform freeware tool for digital reconstruction of neuronal arborizations from image stacks. Neuroinformatics 3:343–360.

Butovsky O, Ziv Y, Schwartz A, Landa G, Talpalar AE, Pluchino S, Martino G, Schwartz M. 2006. Microglia activated by IL-4 or IFN-gamma differentially induce neurogenesis and oligodendrogenesis from adult stem/progenitor cells. Mol Cell Neurosci 31:149–160.

Chen H, Chopp M, Schultz L, Bodzin G, Garcia JH. 1993. Sequential neuronal and astrocytic changes after transient middle cerebral artery occlusion in the rat. J Neurol Sci 118:109–106.

Clausen BH, Lambertsen KL, Babcock AA, Holm TH, Dagnaes-Hansen F, Finsen B. 2008. Interleukin-1beta and tumor necrosis factor-alpha are expressed by different subsets of microglia and macrophages after ischemic stroke in mice. J Neuroinflamm 5:46.

Corsini NS, Sancho-Martinez I, Laudenklos S, Glagow D, Kumar S, Letellier E, Koch P, Teodorczyk M, Kleber S, Klussmann S, Wiestler B, Brustle O, Mueller W, Gieffers C, Hill O, Thiemann M, Seedorf M, Gretz N, Sprengel R, Celikel T, Martin-Villalba A. 2009. The death receptor CD95 activates adult neural stem cells for working memory formation and brain repair. Cell Stem Cell 5:178–190.

Delgado S, Sheremata WA. 2006. The role of $CD4^+$ T-cells in the development of MS. Neurol Res 28:245–249.

Hurn PD, Subramanian S, Parker SM, Afentoulis ME, Kaler LJ, Vandenbark AA, Offner H. 2007. T- and B-cell-deficient mice with experimental stroke have reduced lesion size and inflammation. J Cereb Blood Flow Metab 27:1798–1805.

Ito D, Tanaka K, Suzuki S, Dembo T, Fukuuchi Y. 2001. Enhanced expression of Iba1, ionized calcium-binding adapter molecule 1, after transient focal cerebral ischemia in rat brain. Stroke 32:1208–1215.

Itoh T, Satou T, Hashimoto S, Ito H. 2005. Isolation of neural stem cells from damaged rat cerebral cortex after traumatic brain injury. Neuroreport 16:1687–1691.

Jakubs K, Bonde S, Iosif RE, Ekdahl CT, Kokaia Z, Kokaia M, Lindvall O. 2008. Inflammation regulates functional integration of neurons born in adult brain. J Neurosci 28:12477–12488.

Kitano H, Nishimura H, Tachibana H, Yoshikawa H, Matsuyama T. 2004. ORP150 ameliorates ischemia/reperfusion injury from middle cerebral artery occlusion in mouse brain. Brain Res 1015:122–128.

Kriegstein A, Alvarez-Buylla A. 2009. The glial nature of embryonic and adult neural stem cells. Annu Rev Neurosci 32:149–184.

Lambertsen KL, Clausen BH, Babcock AA, Gregersen R, Fenger C, Nielsen HH, Haugaard LS, Wirenfeldt M, Nielsen M, Dagnaes-Hansen F, Bluethmann H, Faergeman NJ, Meldgaard M, Deierborg T, Finsen B. 2009. Microglia protect neurons against ischemia by synthesis of tumor necrosis factor. J Neurosci 29:1319–1330.

Liesz A, Suri-Payer E, Veltkamp C, Doerr H, Sommer C, Rivest S, Giese T, Veltkamp R. 2009. Regulatory T cells are key cerebroprotective immunomodulators in acute experimental stroke. Nat Med 15:192–199.

Liu T, McDonnell PC, Young PR, White RF, Siren AL, Hallenbeck JM, Barone FC, Feurestein GZ. 1993. Interleukin-1 beta mRNA expression in ischemic rat cortex. Stroke 24:1746–1750; discussion 1750–1741.

Lorke DE, Ip CW, Schumacher U. 2008. Increased number of microglia in the brain of severe combined immunodeficient (SCID) mice. Histochem Cell Biol 130:693–697.

Mannick JB, Hausladen A, Liu L, Hess DT, Zeng M, Miao QX, Kane LS, Gow AJ, Stamler JS. 1999. Fas-induced caspase denitrosylation. Science 284:651–654.

Matsushita K, Matsuyama T, Nishimura H, Takaoka T, Kuwabara K, Tsukamoto Y, Sugita M, Ogawa S. 1998. Marked, sustained expression of a novel 150-kDa oxygen-regulated stress protein, in severely ischemic mouse neurons. Brain Res Mol Brain Res 60:98–106.

Mezey E, Key S, Vogelsang G, Szalayova I, Lange GD, Crain B. 2003. Transplanted bone marrow generates new neurons in human brains. Proc Natl Acad Sci U S A 100:1364–1369.

Morgan MJ, Kim YS, Liu ZG. 2009. Membrane-bound Fas ligand requires RIP1 for efficient activation of caspase-8 within the death-inducing signaling complex. J Immunol 183:3278–3284.

Mukherji B, Guha A, Chakraborty NG, Sivanandham M, Nashed AL, Sporn JR, Ergin MT. 1989. Clonal analysis of cytotoxic and regulatory T cell responses against human melanoma. J Exp Med 169:1961–1976.

Mukherji B, Chakraborty NG, Sivanandham M. 1990. T-cell clones that react against autologous human tumors. Immunol Rev 116:33–62.

Nakagomi T, Taguchi A, Fujimori Y, Saino O, Nakano-Doi A, Kubo S, Gotoh A, Soma T, Yoshikawa H, Nishizaki T, Nakagomi N, Stern DM, Matsuyama T. 2009. Isolation and characterization of neural stem/progenitor cells from post-stroke cerebral cortex in mice. Eur J Neurosci 29:1842–1852.

Niho Y, Asano Y. 1998. Fas/Fas ligand and hematopoietic progenitor cells. Curr Opin Hematol 5:163–165.

Nishi T, Maier CM, Hayashi T, Saito A, Chan PH. 2005. Superoxide dismutase 1 overexpression reduces MCP-1 and MIP-1 alpha expression after transient focal cerebral ischemia. J Cereb Blood Flow Metab 25:1312–1324.

Okano H, Sawamoto K. 2008. Neural stem cells: involvement in adult neurogenesis and CNS repair. Philos Trans R Soc Lond B Biol Sci 363:2111–2122.

O'Reilly LA, Tai L, Lee L, Kruse EA, Grabow S, Fairlie WD, Haynes NM, Tarlinton DM, Zhang J-G, Belz GT, Smyth MJ, Bouillet P, Robb L, Strasser A. 2009. Membrane-bound Fas ligand only is essential for Fas-induced apoptosis. Nature 461:659–663.

Popovich PG, Longbrake EE. 2008. Can the immune system be harnessed to repair the CNS? Nat Rev Neurosci 9:481–493.

Rasley A, Tranguch SL, Rati DM, Marriott I. 2006. Murine glia express the immunosuppressive cytokine, interleukin-10, following exposure to *Borrelia burgdorferi* or *Neisseria meningitidis*. Glia 53:583–592.

Taguchi A, Soma T, Tanaka H, Kanda T, Nishimura H, Yoshikawa H, Tsukamoto Y, Iso H, Fujimori Y, Stern DM, Naritomi H, Matsuyama T. 2004. Administration of $CD34^+$ cells after stroke enhances neurogenesis via angiogenesis in a mouse model. J Clin Invest 114:330–338.

Taguchi A, Wen Z, Myojin K, Yoshihara T, Nakagomi T, Nakayama D, Tanaka H, Soma T, Stern DM, Naritomi H, Matsuyama T. 2007. Granulocyte colony-stimulating factor has a negative effect on stroke outcome in a murine model. Eur J Neurosci 26:126–133.

Uno H, Matsuyama T, Akita H, Nishimura H, Sugita M. 1997. Induction of tumor necrosis factor-alpha in the mouse hippocampus following transient forebrain ischemia. J Cereb Blood Flow Metab 17:491–499.

Van Beek J, Chan P, Bernaudin M, Petit E, MacKenzie ET, Fontaine M. 2000. Glial responses, clusterin, and complement in permanent focal cerebral ischemia in the mouse. Glia 31:39–50.

Yilmaz G, Arumugam TV, Stokes KY, Granger DN. 2006. Role of T lymphocytes and interferon-gamma in ischemic stroke. Circulation 113:2105–2112.

Ann Nucl Med (2010) 24:629–638
DOI 10.1007/s12149-010-0421-7

REVIEW ARTICLE

Nuclear neuroimaging in acute and subacute ischemic stroke

Naohiko Oku · Toru Kashiwagi · Jun Hatazawa

Received: 21 May 2010 / Accepted: 12 August 2010 / Published online: 16 October 2010

Abstract Neuroimaging in ischemic stroke continues to be one of the most developing fields in nuclear medicine. Many studies have established the efficacy of blood flow and metabolism measurements in acute ischemic stroke. Although the release of recombinant tissue plasminogen activator in clinical practice has minimized the use of SPECT or PET in the first few hours of ischemic stroke onset, implementing these techniques into a set of initial examinations is still beneficial to exclude risky patients for reperfusion therapy beyond several hours after onset. Rescuing of viable tissue suffering ischemic penumbra is an important target of early therapeutic strategy. Ischemic penumbra can be visualized by means of perfusion imaging, central type benzodiazepine receptor imaging, and hypoxy imaging. In the later phase of subacute ischemic stroke, inflammation and apoptosis can be visualized by means of peripheral-type benzodiazepine receptor imaging and annexin V imaging, respectively. Imaging of the penumbra and cellular responses will help evaluate the effects of drugs and interventions for ischemic stroke, suggesting its potential as a marker of the efficacy of future therapeutic regimens.

Keywords Neuroimaging · Stroke · Penumbra · SPECT · PET

N. Oku (✉) · T. Kashiwagi
Nuclear Medicine and PET Center, Hyogo College of Medicine, 1-1 Mukogawa, Nishinomiya 663-8501, Japan
e-mail: okun@hyo-med.ac.jp

J. Hatazawa
Department of Nuclear Medicine and Tracer Kinetics, Osaka University Graduate School of Medicine, 2-2 Yamadaoka, Suita 565-0871, Japan

Introduction

Neuroimaging in ischemic stroke continues to be one of the most developing fields in nuclear medicine. Researchers have developed imaging techniques for regional cerebral blood flow (rCBF), regional cerebral metabolism, neuronal integrity, and molecular response in ischemic stroke. Owing to the development of radiopharmaceuticals and techniques such as positron emission tomography (PET) and single-photon emission computed tomography (SPECT), much knowledge of rCBF and metabolism in healthy and pathologic human brains has been accumulated. These imaging modalities allow us to understand the pathophysiology in ischemic stroke and help determine the diagnosis, treatment, and management. Measurement of rCBF and metabolism plays critical roles in acute ischemic stroke because they directly correlate with the prognosis of functional recovery [1–4]. In the past 3 decades, many studies using SPECT or PET evaluated the cerebral hemodynamic or metabolic changes in acute ischemic stroke, and the usefulness of rCBF and metabolism measurement was established.

However, the release of recombinant tissue plasminogen activator (tPA) in clinical practice [5] has minimized the number of chances to measure the hemodynamic changes by means of SPECT or PET within a few hours of ischemic stroke onset. Under governmental safety regulations, tPA must be intravenously administered as soon as possible within the first 3 h of onset [6]. In the usual circumstances, there is insufficient time to perform SPECT or PET before tPA administration. Taking everything into consideration, recent guidelines for acute stroke imaging in Japan [7] do not recommend rCBF SPECT examination in the first 3 h of onset.

Today, many methods for imaging specific molecules of cellular function have been developed. These techniques

can visualize hypoxia, neuronal integrity, apoptosis, inflammation, and so on. In this review, we focused on the role of nuclear neuroimaging in clinically acute and subacute ischemic stroke.

Hemodynamic changes in acute ischemic stroke

A multicenter PET study in Japan [8] showed that the overall mean ± SD values in the cerebral cortex of healthy human subjects were as follows: rCBF = 44.4 ± 6.5 ml/100 ml/min; regional cerebral metabolic rate of oxygen ($rCMRO_2$) = 3.3 ± 0.5 ml/100 ml/min; regional cerebral blood volume (rCBV) = 3.8 ± 0.7 ml/100 ml; regional oxygen extraction fraction (rOEF) = 0.44 ± 0.06. In the acute phase of ischemic stroke, uncoupling between rCBF and metabolism is often observed. Many investigations using PET on ischemic stroke had proven the dynamic changes of rCBF and $rCMRO_2$. These studies are well summarized elsewhere [9]. With acute obstruction of a cerebral artery, rCBF dramatically falls to below the critical level, whereas the reduction of $rCMRO_2$ in the ischemic lesion is relatively mild. This condition is called "misery perfusion" [10], in which rOEF and rCBV increase [11].

In some cases, activation of the intrinsic thrombolytic system leads to spontaneous recanalization within a few hours to days. If the damage of the ischemic lesion is limited, this phenomenon allows ischemic tissues to survive infarction. Regarding the clinical manifestations, there may appear a rapid neurological recovery called "spectacular shrinking deficit" [12]. Minematsu et al. [13] reported that this phenomenon occurred in 12% of major hemispheric syndrome. Under this condition, rCBF in the lesion becomes higher than that in normal tissue. This phenomenon is called "early post-ischemic hyperperfusion" [14, 15]. Baird et al. [16] and Marchal et al. [17] reported that the early post-ischemic hyperperfusion correlated with smaller infarcts on X-ray computed tomography (CT).

Unfortunately, in most cases, the ischemic lesion is threatened by irreversible neuronal damage. Garcia et al. [18] reported in a rat study that the early neuronal changes in structure began at 30 min after ischemia and were reversible for up to 6 h, but thereafter the changes became irreversible. The threshold of infarction-prone tissue in human is reportedly 10–15 ml/100 ml/min for rCBF and 1.0–1.3 ml/100 ml/min for $rCMRO_2$ [19–21]. The threshold is considered as a function of the intensity and duration of ischemia. Jones et al. [22] stated that the infarction threshold, increased steeply over a few hours to a plateau, below which the tissue structure was irreversibly damaged. Absolute shortage of oxygen supply results in membranous ion pump failure that triggers irreversible neuronal damage and cytotoxic edema. Release of cytotoxic substances such as excitatory neurotransmitters, reactive oxygen species, and prostanoids augments the damage of the surrounding ischemic cells [23], and the subsequent damage of the vascular endothelium causes vasogenic edema [24]. In this condition, therapeutic recanalization is highly risky because it may trigger fatal intracerebral hemorrhage. Thus, it is of clinical value in the initial treatment for acute stroke to distinguish the salvageable tissue from infarct-prone tissue.

Identifying risky patients for early reperfusion therapy

Although PET is a powerful tool to identify the hemodynamic and metabolic crises occurring in ischemic lesions, inclusion of PET as a routine examination in the initial treatment for acute stroke is limited because of the need for manpower and time. Instead of PET, many reports have supported the clinical usefulness of perfusion SPECT in predicting the prognosis of ischemic lesions in acute stroke. Early studies have demonstrated the clinical advantage of perfusion SPECT in predicting the prognosis of stroke patients as compared with CT [25–28]. As was expected, a deeper or larger ischemic lesion predicted a poorer functional outcome. In the past 2 decades, many studies using perfusion SPECT [2, 29–35] successfully demonstrated the ischemic threshold in acute stroke (Table 1). These studies commonly demonstrated that most of the ischemic lesions under a certain rCBF level or most of the hyperemic lesions would progress to complete infarction. Shimosegawa et al. [29] reported in their study on acute ischemic stroke within 6 h of onset that infarction could be predicted by a lesion-to-contralateral radioactivity ratio of 0.6 or smaller. Some studies [32, 34, 35] successfully demonstrated the relationships among the progress of infarction, severity of ischemia, and time from onset. Ueda et al. [30, 32] suggested that the ischemic lesion under a certain rCBF level (35% of ipsilateral cerebellar hemisphere) would suffer intracerebral hemorrhage after the application of thrombolytic therapy. Accordingly, quantitative rCBF measurement seems unnecessary because the semi-quantitative methods such as lesion to normal contralateral ratio or lesion to cerebellum ratio can reliably distinguish stroke-prone lesions. However, the rCBF threshold of the infarct-prone lesion exhibited some differences among the studies. These may depend on various conditions such as the type of radiopharmaceutical used, procedure of imaging technique, time-range from onset, type of stroke, patients' age distribution, and therapy.

Taking these results into consideration, rCBF evaluation using SPECT seems beneficial in predicting the highly risky

Table 1 Flow thresholds in % of reference (or ml/100 ml/min) for infarct-prone tissue in acute stroke as measured by SPECT

Authors	Tracer	Number of patients	Stroke types	Time from onset (h)	Threshold	References
Shimosegawa[a]	HMPAO	31	CE, AT	1.5–5.7	60%, 140%<	[29]
Ueda[a]	HMAPO	20	CE, AT	<7.5	35% for ICH	[30]
Ueda[a]	HMPAO	30	CE, AT	2–12	35% for ICH 55% for INF	[32]
Berrouschot	ECD	82	MCA stroke, TIA	<6	70%	[31]
Watanabe	ECD	20	CE	1–12	20 ml/100 ml/min	[28]
Mahagne	ECD	24	MCA stroke	4–12	40%	[2]
Ogasawara[a]	ECD	28	MCA ES	3–6	55%	[33]
Iseda[a]	ECD	19	MCA OC	2.5–8	34–50% (≦3 h) 50% (>3 h)	[34]
Hirano	HMPAO	53	ES	0.8–6	30–60% (≦1 h) 60% (>1 h)	[35]

HMPAO ^{99m}Tc-hexamethylpropyleneamine oxime, *ECD* ^{99m}Tc-ethyl cysteinate dimer, *CE* cardioembolic, *AT* atherothrombotic, *MCA* middle cerebral artery, *TIA* transient ischemic attack, *ES* embolic stroke, *OC* occlusion, *ICH* intracranial hemorrhage, *INF* infarction

[a] Include thrombolytic therapy

patient for reperfusion therapy. However, unfortunately, perfusion CT or perfusion/diffusion magnetic resonance imaging (MRI) has been developed as a diagnostic tool for acute stroke before deciding on therapy. These techniques can predict the ischemic core and penumbral area to a considerable degree [36–38]. Currently, conducting perfusion SPECT study in a set of initial examinations for acute stroke may be limited to patients who are unsuitable for perfusion CT or MRI. Perfusion SPECT as well as short-run ^{15}O-PET methods [39–41] may contribute to the therapeutic strategies in patients with stroke more than several hours after onset, in patients with unknown time of onset (e.g. 'awakening stroke'), and in patients with progressing stroke.

Imaging ischemic penumbra

In the acute phase of ischemic stroke, it is suggested that the ischemic core is surrounded by "ischemic penumbra" [21, 42]. The ischemic penumbra is characterized by hypoperfusion and functionally impaired neurons without structural deterioration (Fig. 1). Although the area of ischemic penumbra is expected to survive, it is fragile and often progresses to complete infarction. The conversion of penumbra into infarction is a dynamic, time-dependent process spreading from the ischemic core to its border [43–47]. Thus, the rescue of viable tissue suffering ischemic penumbra is an important target of early therapeutic intervention.

Imaging penumbra by perfusion and metabolism

Among some potential methods to visualize the ischemic penumbra, ^{15}O-PET has been considered the golden

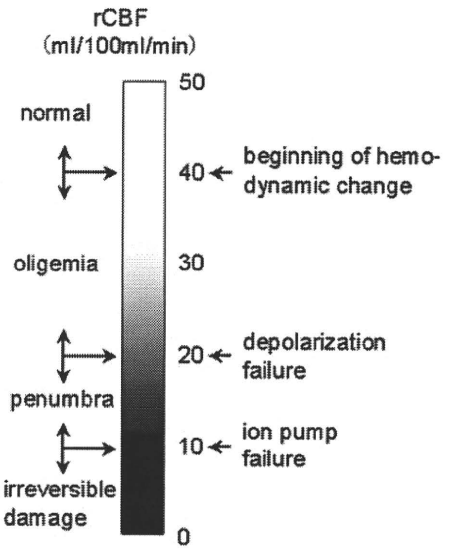

Fig. 1 Schematic representation of ischemic thresholds as measured by the regional cerebral blood flow (rCBF). The *gray level* indicates the risk of neuronal death, the *white* indicates no risk, and the *black* is lethal

standard. The quantitative measurement of rCBF, $rCMRO_2$, rOEF, and rCBV allows an independent assessment of perfusion and oxygen metabolism, and demonstrates the uncoupling of these parameters. This approach has tried to visualize the ischemic penumbra by detecting lesions with hypoperfusion, mild hypometabolism, and elevated rOEF and rCBV. Many investigators [19, 20, 45–47] have tried to visualize the localization of ischemic penumbra by using PET. These meticulous clinical PET studies in acute ischemic stroke revealed that the penumbral range was 7–22 ml/100 ml/min for rCBF and above 1.3-1.6 ml/100 ml/min for

Table 2 Flow and metabolic thresholds in ml/100 ml/min (or % of reference) for ischemic penumbra

Author	Tracer	Number of patients	Time from onset (h)	CBF (ml/100 ml/min)	$CMRO_2$ (ml/100 ml/min)	References
Powers	^{15}O	50	<6	15–19	>1.3	[19]
Hakim	^{15}O	14	<48	12–18		[45]
Higano	^{15}O	9	7–32	10–17	>1.6	[20]
Furlan	^{15}O	26	<18	7–17		[48]
Marchal	^{15}O	8	7–17	10–22	>1.4	[49]
Watanabe	ECD	20	1–12	>20		[28]
Hatazawa	HMPAO	9	2.5–8.4	>40%		[50]
Mahagne	ECD	18	4.5–12	40–80%		[51]

CBF cerebral blood flow, *$CMRO_2$* cerebral metabolic rate of oxygen, *HMPAO* ^{99m}Tc-hexamethylpropyleneamine oxime, *ECD* ^{99m}Tc-ethyl cysteinate dimer

$rCMRO_2$ (Table 2). Elevated rOEF or rCBV seemed to be less sensitive [48, 50, 52].

Perfusion SPECT is also a practical candidate for the detection of ischemic penumbra in the acute phase. Among tracers, ^{99m}Tc-hexamethylpropyleneamine oxime (HMPAO) and ^{99m}Tc-ethyl cysteinate dimer (ECD) are frequently selected because of their rapid availability. Some meticulous clinical studies [28, 50, 51] demonstrated that the lower threshold of penumbra was 20 ml/100 ml/min or 40% of the contralateral normal region (Table 2). This threshold included the range of rCBF when the ischemic lesion eventually progressed to infarction. The upper threshold of penumbra on using SPECT seemed to be 55–80% of the contralateral normal region [29–32, 51].

Imaging penumbra by neuronal integrity

The second approach for imaging the ischemic penumbra is a central-type benzodiazepine receptor (cBZR) imaging. The cBZR is a postsynaptic [53], purely neuronal receptor that distributes profusely in the cerebral cortex but not in the cerebellar cortex and subcortical structures [54, 55]. The expression of cBZR on the neuronal membrane was found to be a sensitive marker of neuronal integrity [56], and therefore cBZR ligand could be sufficiently sensitive to identify early irreversible neuronal injury [57]. In acute stroke patients, the final cortical infarctions were predicted on the early ^{11}C-flumazenil (FMZ) images [58]. Heiss et al. [59] first reported that the combination of ^{15}O-water and FMZ PET was a potential marker of predicting the clinical outcome of penumbra. The lower threshold of FMZ binding for irreversible tissue damage and the upper threshold of penumbral rCBF were 3.4 times the mean of the normal white matter and 14.1 ml/100 ml/min, respectively. However, in 20.5% of the final infarcts, CBF was in the penumbral range while FMZ binding was above the critical threshold [59]. In a recent voxel-based analysis of FMZ PET in acute stroke [60], rescued penumbra seemed to be affected by selective neuronal death to various degrees according to the severity of the initial hypoperfusion. There were some similar studies [61–63] of ischemic stroke using ^{123}I-iomazenil (IMZ), a single photon analog of FMZ, and SPECT. Hatazawa et al. [61] and Nakagawara et al. [62] reported that the peri-infarct or reperfused areas where the structures appeared intact were affected by neuronal loss to various degrees. Dong et al. [63] and Saur et al. [64] observed in patients with subcortical or striate-capsular infarctions that the overlying normal-appearing cortices were affected by mild to moderate neuronal loss. These findings may also contribute to distinguish neuronal loss from diaschisis (Fig. 2). However, these SPECT studies were limited to a relatively late phase, from 4 days to 23 months after ictus. The clinical value of IMZ SPECT in acute ischemic stroke within several hours of ictus awaits further investigations.

Imaging penumbra by hypoxic markers

Markers of hypoxic tissue have been also investigated to test their capacity to visualize penumbra. Misonidazole, a derivative of nitroimidazole, is trapped only by the hypoxic cells with enzymatic activities [65]. In the experimental animal stroke model, tritium [66] or ^{18}F [67] labeled misonidazole (FMISO) appeared to be a diagnostic indicator of hypoxic but viable tissue. Read and colleagues [68–70] have demonstrated the dynamic changes occurring in hypoxic tissue using FMISO and PET in acute stroke patients. Hypoxic tissue was detected in 9 of 13 patients examined within 48 h of ictus, and was generally distributed in the peripheries of the infarct and adjacent peri-infarcted area. The increased FMISO uptake disappeared in the late phase indicating progression to infarction or survival [68]. Furthermore, the initial stroke severity correlated significantly with the initially affected volume detected by FMISO [69]. These hypoxic but viable tissues were observed in the central region of the infarct within 6 h of ictus as compared with the tissues examined later, when they were distributed in the periphery or external to the infarct [70]. Spratt et al. [71]

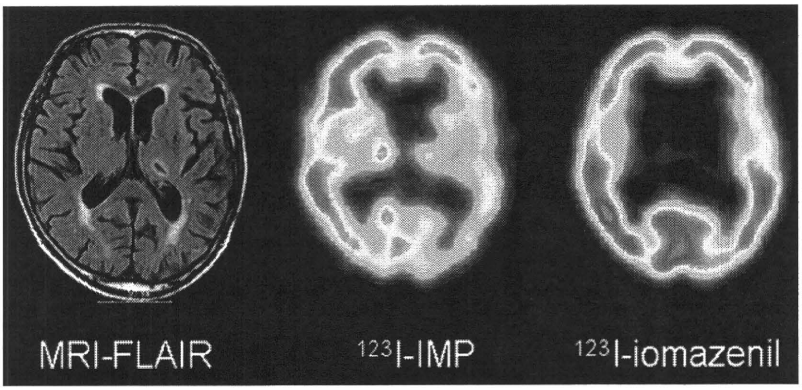

Fig. 2 Fluid-attenuated inversion recovery image of magnetic resonance imaging (MRI-FLAIR) and multitracer SPECT images in a patient with subacute left thalamic lacunar infarction without major artery obstruction. There is no apparent cortical lesion except for mild periventricular hyperintensity on MRI-FLAIR. Perfusion SPECT using ^{123}I-IMP demonstrates mild hypoperfusion in the left hemispheric cortices and the thalamus. Central benzodiazepine receptor SPECT imaging using ^{123}I-iomazenil demonstrates slightly reduced accumulation in the left frontal and temporal cortices and mildly reduced accumulation in the left occipital cortex. This discrepancy between perfusion and ^{123}I-iomazenil accumulation in the left frontal and temporal cortices suggests diaschisis because neuron integrity seems to be preserved except in the left occipital cortex. In the left occipital cortex, there may be neuronal damage for some unknown reason

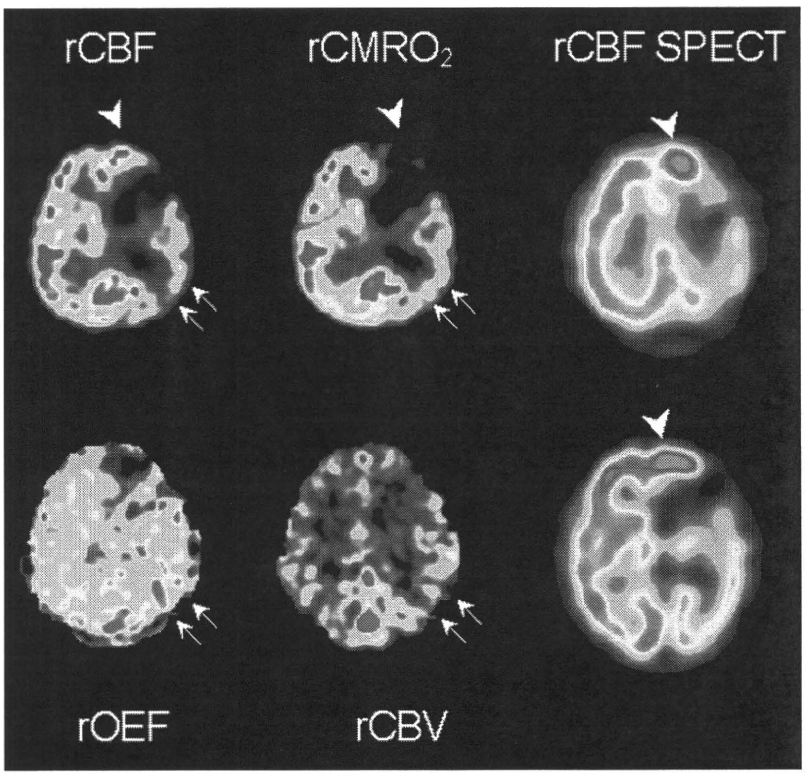

Fig. 3 A case of subacute left hemispheric stroke due to left internal carotid occlusion. Oxygen-15 gas PET study (*left* and *center column*) clearly demonstrates luxury perfusion in the left frontal cortex (*arrowhead*). Perfusion SPECT using ^{99m}Tc-HMPAO (*right column*) demonstrates hyperperfusion and hyperfixation in the same region (*arrowhead*). Misery perfusion is also seen in the left temporo-occipital region (*small arrows*)

demonstrated in the animal stroke model that ^{3}H-FMISO binding did not occur after effective reperfusion, despite histological injury induced by the preceding ischemia. They suggested that FMISO uptake was indicative of ongoing tissue hypoxia. Although FMISO is a potential marker of hypoxic crisis in the ischemic penumbra, its application in acute stroke is limited because the preparation of FMISO is not readily available.

Hemodynamic changes in subacute ischemic stroke

In the subacute phase (>48 h) of ischemic stroke, most of the ischemic lesions will progress to complete infarction [43–46]. The mismatch between perfusion and metabolism gradually disappears with time [43, 44]. Although the fate of ischemic lesion has almost been fixed, spontaneous reperfusion may still occur with considerable frequency.

Bowler et al. [72] reported that visually apparent reperfusion on ^{99m}Tc-HMPAO SPECT occurred in 28% of acute stroke patients with a mean delay of 5.8 days, but was associated with clinical improvement in only 2%. In this condition, the mismatch between perfusion and metabolism appears again (Fig. 3). This phenomenon is called "luxury perfusion" or "hyperperfusion" [15]. Luxury perfusion is defined as an excessive rCBF as compared with the metabolic demand, and so it is not always higher than the normal value. Accordingly, this is properly diagnosed by measuring both rCBF and metabolism using PET. Hyperperfusion is a simple phenomenon in which rCBF becomes higher than the normal value irrespective of metabolism, and it can to be detected by SPECT.

Although there are some small differences between the distribution of ^{99m}Tc-labeled perfusion SPECT tracers [73, 74], sensitivity and specificity are almost the same in predicting chronic ischemic lesions. In the acute or subacute phase of stroke, there are some noticeable phenomena on examining rCBF using ^{99m}Tc-labeled SPECT tracers. Sperling et al. [75] noticed a "hyperfixation" phenomenon of ^{99m}Tc-HMPAO in subacute ischemic stroke. They reported that the accumulation of ^{99m}Tc-HMPAO in the subacute ischemic lesion might be higher than that expected from rCBF as measured by quantitative ^{133}Xe inhalation SPECT. The main mechanisms of hyperfixation are considered to be vasodilatation [76], cell membrane disruption [77], mitochondrial damage [78], neovascularization, and blood brain barrier (BBB) disruption [79]. Unlike other SPECT tracers, ^{99m}Tc-ECD is characterized by reduced accumulation in tissue with reflow hyperperfusion [80–84]. Studies comparing ^{99m}Tc-ECD SPECT with PET [81, 83] suggested that the accumulation of ^{99m}Tc-ECD depended on the regional oxygen metabolism. This phenomenon was explained by the property of transformation of ^{99m}Tc-ECD into a hydrophilic form: i.e., retention mechanism, that depended highly on the enzymatic activity [85, 86]. Despite the disadvantage, Ogasawara et al. [84] successfully visualized reflow hyperperfusion in patients with subacute stroke by super-early dynamic ^{99m}Tc-ECD SPECT.

Imaging following cellular responses

Inflammation and apoptosis play crucial roles during ongoing structural or functional rearrangement after ischemic stroke. Imaging of these functions can evaluate the effects of drugs and interventions for ischemic stroke, suggesting its potential role as a marker of efficacy in future therapeutic regimens.

Microglia are the pivot of the intracerebral cytokine network. They are in a resting state and perform homeostatic activity in the healthy central nervous system. Any pathologic processes turn them rapidly into an active state, "activated microglia". Recent studies have shown that the activated microglia had bipolar reactions: one was neurotoxic that eliminated the injured neurons, and the other was neuroprotective that helped the injured neurons recover [87–89]. PK11195 is a potent ligand of peripheral-type benzodiazepine receptors that is specific to the activated microglia [90]. Previous studies [56, 91–95] demonstrated that the activated microglia were seen as early as 3 days after ictus [93] in the peri-infarcted area with [91–94] or without [56, 90, 95] infarcted core involvement. The accumulation of PK11195 was also seen in the chronic phase of stroke and in areas distant from the primary lesion. These studies suggested the functional role of inflammation in Wallerian degeneration [96], and possible therapeutic strategies that might extend beyond the traditional therapeutic time window.

Apoptosis is an important mechanism of cell death which works in keeping homeostasis as well as removal of damaged cells or uncontrolled cells. Although apoptosis is usually an irreversible process, some neuroprotective substances can reportedly interrupt it. The triggers of apoptosis are cell stresses, such as ischemia, excitatory neurotransmitters, cytokines, endoplasmic reticulum stress, and so on. Recent studies have demonstrated that even a brief ischemic event might trigger apoptosis and that the neurons in the ischemic penumbra would be threatened by apoptosis [97, 98]. In healthy cells, phosphatidylserine (PS) is exclusively localized in the membrane leaflet facing the cytosol (PS asymmetry) [99, 100]. Fadok et al. [101] found the basic phenomenon for a novel apoptosis detection technique by showing that ongoing apoptotic cells expose PS on their outer surface. Annexin V, an endogenous human protein, was found to sensitively bind to the PS-enriched cell surface in a calcium ion-dependent manner [102, 103] (Fig. 4). The use of ^{99m}Tc hydrazine nicotinamide-labeled annexin V (^{99m}Tc-HYNIC-annexinV) has been reported in some clinical investigations of acute ischemic stroke. Blankenberg et al. [104] reported 2 patients with acute ischemic stroke, in whom multifocal annexin V uptake was observed in the region of restricted diffusion on MRI. The uptake resolved in the follow-up study performed 1 month later. Lorberboym et al. [105] reported that abnormal uptake of annexin V occurred in infarcted lesions despite the intact BBB as assessed by ^{99m}Tc-DTPA. Both studies observed annexin V uptake in remote regions of both ipsilateral and contralateral hemispheres to a lesser degree. This phenomenon suggested that diaschisis might cause cell stress via functionally connected interneuronal pathways.

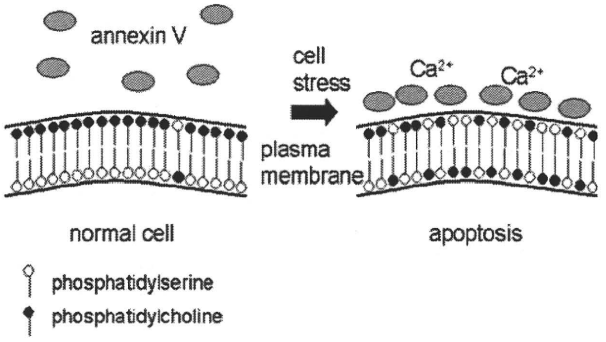

Fig. 4 Illustrative representation of annexin V binding to the apoptotic cell. In the normal cell, phosphatidylserine is exclusively localized in the inner leaflet of the plasma membrane. In the ongoing apoptotic cells, phosphatidylserine begins to move to the outer leaflet of the plasma membrane. Annexin V sensitively binds to phosphatidylserine on the cell surface in a calcium ion-dependent manner

Conclusion

The commercial release of tPA has changed the role of SPECT or PET in acute ischemic stroke. Although perfusion CT or perfusion/diffusion MRI has been developed as a diagnostic tool for acute stroke, conducting perfusion SPECT study in a set of initial examinations may be still beneficial to patients with stroke more than several hours after onset and those with progressing stroke. Short-run ^{15}O-PET methods may also be good candidates for precise evaluation or research purposes.

Imaging of the penumbra and cellular responses will help evaluate the effects of drugs and interventions for ischemic stroke, suggesting its potential as a marker of efficacy in future therapeutic regimens.

References

1. Friedman PJ, Davis G, Allen B. Semi-quantitative SPECT scanning in acute ischaemic stroke. Scand J Rehabil Med. 1993;25:99–105.
2. Mahagne MH, Darcourt J, Migneco O, Fournier JP, Thiercelin D, Ducoeur S, et al. Early ^{99m}Tc-ethylcysteinate dimer brain SPECT patterns in the acute phase of stroke as predictors of neurological recovery. Cerebrovasc Dis. 2000;10:364–73.
3. Alexandrov AV, Ehrlich LE, Bladin CF, Norris JW. Noninvasive assessment of intracranial perfusion in acute cerebral ischemia. J Neuroimaging. 1995;5:76–82.
4. Giubilei F, Lenzi GL, Di Pielo V, Pozzilli C, Pantano P, Bastianello S, et al. Predictive value of brain perfusion single-photon emission computed tomography in acute ischemic stroke. Stroke. 1990;21:895–900.
5. Hacke W, Kaste M, Fieschi C, Toni D, Lesaffre E, von Kummer R, et al. Intravenous thrombolysis with recombinant tissue plasminogen activator for acute hemispheric stroke. The European cooperative acute stroke study (ECASS). JAMA. 1995;274:1017–25.
6. Clark WM, Wissman S, Albers GW, Jhamandas JH, Madden KP, Hamilton S. Recombinant tissue-type plasminogen activator (alteplase) for ischemic stroke 3 to 5 hours after symptom onset: the ATLANTIS study: A randomized controlled trial. JAMA. 1999;282:2019–26.
7. Acute Stroke Imaging Standardization Group-Japan. Procedure guidelines for acute stroke imaging 2007. Tokyo: Nankodo; 2007.
8. Ito H, Kanno I, Fukuda H. Human cerebral circulation: positron emission tomography studies. Ann Nucl Med. 2005;19:65–74.
9. Okazawa H, Kudo T. Clinical impact of hemodynamic parameter measurement for cerebrovascular disease using positron emission tomography and ^{15}O-labeled tracers. Ann Nucl Med. 2009;23:217–27.
10. Baron JC, Bousser MG, Rey A, Guillard A, Comar D, Castaigne P. Reversal of focal "misery-perfusion syndrome" by extra-intra-cranial arterial bypass in hemodynamic cerebral ischemia. A case study with ^{15}O positron emission tomography. Stroke. 1981;12:454–9.
11. Powers WJ, Raichle ME. Positron emission tomography and its application to the study of cerebrovascular disease in man. Stroke. 1985;16:361–76.
12. Mohr JP, Barnett HJM. Classification of ischemic strokes. In: Barnett HJM, Stein BM, Mohr JP, Yatsu FM, editors. Stroke: pathophysiology, diagnosis, and management, vol. 1. New York: Churchill Livingston; 1986. p. 281–91.
13. Minematsu K, Yamaguchi T, Omae T. 'Spectacular shrinking deficit': rapid recovery from a major hemispheric syndrome by migration of an embolus. Neurology. 1992;42:157–62.
14. Olsen TS, Larsen B, Skriver EB, Herning M, Enevoldsen E, Lassen NA. Focal cerebral hyperemia in acute stroke. Incidence, pathophysiology and clinical significance. Stroke. 1981;12:598–607.
15. Marchal G, Young AR, Baron JC. Early postischemic hyperperfusion: pathophysiologic insights from positron emission tomography. J Cereb Blood Flow Metab. 1999;19:467–82.
16. Baird AE, Donnan GA, Austin MC, McKay WJ. Early reperfusion in the 'spectacular shrinking deficit' demonstrated by single-photon emission computed tomography. Neurology. 1995;45:1335–9.
17. Marchal G, Furlan M, Beaudouin V, Rioux P, Hauttement JL, Serrati C, et al. Early spontaneous hyperperfusion after stroke. A marker of favourable tissue outcome? Brain. 1996;119:409–19.
18. Garcia JH, Yoshida Y, Chen H, Li Y, Zhang ZG, Lian J, et al. Progression from ischemic injury to infarct following middle cerebral artery occlusion in the rat. Am J Pathol. 1993;142:623–35.
19. Powers WJ, Grubb RL, Darriet D, Raichle ME. Cerebral blood flow and cerebral metabolic rate of oxygen requirements for cerebral function and viability in humans. J Cereb Blood Flow Metab. 1985;5:600–8.
20. Higano S, Uemura K, Shishido F, Kanno I, Tomura N, Sakamoto K. Evaluation of critically perfused area in acute ischemic stroke for therapeutic reperfusion: a clinical PET study. Ann Nucl Med. 1993;7:167–71.
21. Astrup J, Siesjö BK, Symon L. Thresholds in cerebral ischemia—the ischemic penumbra. Stroke. 1981;12:723–5.
22. Jones TH, Morawetz RB, Crowell RM, Marcoux FW, FitzGibbon SJ, DeGirolami U, et al. Thresholds of focal cerebral ischemia in awake monkeys. J Neurosurg. 1981;54:773–82.
23. Doyle KP, Simon RP, Stenzel-Poore MP. Mechanisms of ischemic brain damage. Neuropharmacology. 2008;55:310–8.
24. Nag S, Manias JL, Stewart DJ. Pathology and new players in the pathogenesis of brain edema. Acta Neuropathol. 2009;118:197–217.

25. Yeh SH, Liu RS, Hu HH, Wong WJ, Lo YK, Lai ZY, et al. Brain SPECT imaging with ^{99m}Tc-hexamethylpropyleneamine oxime in the early detection of cerebral infarction: comparison with transmission computed tomography. Nucl Med Commun. 1986;7:873–8.
26. Hill TC, Holman BL, Lovett R, O'Leary DH, Front D, Magistretti P, et al. Initial experience with SPECT (single-photon computerized tomography) of the brain using N-isopropyl I-123 p-iodoamphetamine: Concise communication. J Nucl Med. 1982;23:191–5.
27. Launes J, Nikkinen P, Lindroth L, Brownell AL, Liewendahl K, Livanainen M. Brain perfusion defect size in SPECT predicts outcome in cerebral infarction. Nucl Med Commun. 1989; 10:891–900.
28. Watanabe Y, Takagi H, Aoki S, Sassa H. Prediction of cerebral infarct sizes by cerebral blood flow SPECT performed in the early acute stage. Ann Nucl Med. 1999;13:205–10.
29. Shimosegawa E, Hatazawa J, Inugami A, Fujita H, Ogawa T, Aizawa Y, et al. Cerebral infarction within six hours of onset: prediction of completed infarction with technetium-99m-HMPAO SPECT. J Nucl Med. 1994;35:1097–103.
30. Ueda T, Hatakeyama T, Kumon Y, Sakaki S, Uraoka T. Evaluation of risk of hemorrhagic transformation in local intra-arterial thrombolysis in acute ischemic stroke by initial SPECT. Stroke. 1994;25:298–303.
31. Berrouschot J, Barthel H, Hesse S, Köster J, Knapp WH, Schneider D. Differentiation between transient ischemic attack and ischemic stroke within the first six hours after onset of symptoms by using ^{99m}Tc-ECD-SPECT. J Cereb Blood Flow Metab. 1998;18:921–9.
32. Ueda T, Sakaki S, Yuh WTC, Nochide I, Ohta S. Outcome in acute stroke with successful intra-arterial thrombolysis and predictive value of initial single-photon emission-computed tomography. J Cereb Blood Flow Metab. 1999;19:99–108.
33. Ogasawara K, Ogawa A, Doi M, Konno H, Suzuki M, Yoshimoto T. Prediction of acute embolic stroke outcome after local intraarterial thrombolysis: Value of pretreatment and posttreatment ^{99m}Tc-ethyl cysteinate dimer single photon emission computed tomography. J Cereb Blood Flow Metab. 2000;20:1579–86.
34. Iseda T, Nakano S, Yano T, Suzuki Y, Wakisaka S. Time-threshold curve determined by single photon emission CT in patients with acute middle cerebral artery occlusion. AJNR Am J Neuroradiol. 2002;23:572–6.
35. Hirano T, Yonehara T, Inatomi Y, Hashimoto Y, Uchino M. Presence of early ischemic changes on computed tomography depends on severity and the duration of hypoperfusion. A single photon emission-computed tomographic study. Stroke. 2005; 36:2601–8.
36. Gasparotti R, Grassi M, Mardighian D, Frigerio M, Pavia M, Liserre R, et al. Perfusion CT in patients with acute ischemic stroke treated with intra-arterial thrombolysis: predictive value of infarct core size on clinical outcome. AJNR Am J Neuroradiol. 2009;30:722–7.
37. Lansberg MG, Thijs VN, Bammer R, Olivot JM, Marks MP, Wechsler LR, et al. The MRA-DWI mismatch identifies patients with stroke who are likely to benefit from reperfusion. Stroke. 2008;39:2491–6.
38. Takasawa M, Jones PS, Guadagno JV, Christensen S, Fryer TD, Harding S, et al. How reliable is perfusion MR in acute stroke? Validation and determination of the penumbra threshold against quantitative PET. Stroke. 2008;39:870–7.
39. Ibaraki M, Shimosegawa E, Miura S, Takahashi K, Ito H, Kanno I, et al. PET measurements of CBF, OEF, and $CMRO_2$ without arterial sampling in hyperacute ischemic stroke: method and error analysis. Ann Nucl Med. 2004;18:35–44.
40. Kobayashi M, Okazawa H, Tsuchida T, Kawai K, Fujibayashi Y, Yonekura Y. Diagnosis of misery perfusion using noninvasive ^{15}O gas PET. J Nucl Med. 2006;47:1581–6.
41. Kobayashi M, Kudo T, Tsujikawa T, Isozaki M, Arai Y, Fujibayashi Y, et al. Shorter examination method for the diagnosis of misery perfusion with count-based oxygen extraction fraction elevation in ^{15}O-gas PET. J Nucl Med. 2008;49:242–6.
42. Olsen TS, Larsen B, Herning M, Skriver EB, Lassen NA. Blood flow and vascular reactivity in collaterally perfused brain tissue. Evidence of an ischemic penumbra in patients with acute stroke. Stroke. 1983;14:332–41.
43. Wise RJ, Bernardi S, Frackowiak RS, Legg NJ, Jones T. Serial observations on the pathophysiology of acute stroke. The transition from ischaemia to infarction as reflected in regional oxygen extraction. Brain. 1983;106:197–222.
44. Heiss WD, Huber M, Fink GR, Herholz K, Pietrzyk U, Wagner R, et al. Progressive derangement of periinfarct viable tissue in ischemic stroke. J Cereb Blood Flow Metab. 1992;12:193–203.
45. Hakim AM, Evans AC, Berger L, Kuwabara H, Worsley K, Marchal G, et al. The effect of nimodipine on the evolution of human cerebral infarction studied by PET. J Cereb Blood Flow Metab. 1989;9:523–34.
46. Heiss WD, Graf R, Wienhard K, Löttgen J, Saito R, Fujita T, et al. Dynamic penumbra demonstrated by sequential multitracer PET after middle cerebral artery occlusion in cats. J Cereb Blood Flow Metab. 1994;14:892–902.
47. Baron JC. Mapping of the ischaemic penumbra with PET: Implications for acute stroke treatment. Cerebrovasc Dis. 1999;9:193–201.
48. Furlan M, Marchal G, Viader F, Derlon JM, Baron JC. Spontaneous neurological recovery after stroke and the fate of the ischemic penumbra. Ann Neurol. 1996;40:216–26.
49. Marchal G, Beaudouin V, Rioux P, de la Sayette V, Le Doze F, Viader F, et al. Prolonged persistence of substantial volumes of potentially viable brain tissue after stroke. A correlative PET-CT study with voxel-based data analysis. Stroke. 1996;27:599–606.
50. Hatazawa J, Shimosegawa E, Toyoshima H, Ardekani BA, Suzuki A, Okudera T, et al. Cerebral blood volume in acute brain infarction. A combined study with dynamic susceptibility contrast MRI and ^{99m}Tc-HMPAO-SPECT. Stroke. 1999;30:800–6.
51. Mahagne MH, David O, Darcourt J, Migneco O, Dunac A, Chatel M, et al. Voxel-based mapping of cortical ischemic damage using Tc-99m L, L-ethyl cysteinate dimer SPECT in acute stroke. J Neuroimaging. 2004;14:23–32.
52. Marchal G, Benali K, Iglesias S, Viader F, Derlon JM, Baron JC. Voxel-based mapping of irreversible ischaemic damage with PET in acute stroke. Brain. 1999;122:2387–400.
53. Connors BW, Malenka RC, Silva LR. Two inhibitory postsynaptic potentials, and $GABA_A$ and $GABA_B$ receptor-mediated responses in neocortex of rat and cat. J Physiol. 1988; 406:443–68.
54. d'Argy R, Persson A, Sedvall G. A quantitative cerebral and whole body autoradiographic study of a intravenously administered benzodiazepine antagonist 3H-Ro 15-1788 in mice. Psychopharmacology. 1987;92:8–13.
55. Mazière M, Hantraye P, Kaijima M, Dodd R, Guibert B, Prenant C, et al. Visualization by positron emission tomography of apparent regional heterogeneity of central type benzodiazepine receptors in the brain of living baboons. Life Sci. 1985; 36:1609–16.
56. Sette G, Baron JC, Young AR, Miyazawa H, Tillet I, Barré L, et al. In vivo mapping of brain benzodiazepine receptor changes by positron emission tomography after focal ischemia in the anesthetized baboon. Stroke. 1993;24:2046–57.
57. Schwartz RD, Yu X, Wagner J, Ehrmann M, Mileson BE. Cellular regulation of the benzodiazepine/GABA receptor:

arachidonic acid, calcium, and cerebral ischemia. Neuropsychopharmacology. 1992;6:119–25.
58. Heiss WD, Grond M, Thiel A, Ghaemi M, Sobesky J, Rudolf J, et al. Permanent cortical damage detected by flumazenil positron emission tomography in acute stroke. Stroke. 1998; 29:454–61.
59. Heiss WD, Kracht LW, Thiel A, Grond M, Pawlik G. Penumbral probability thresholds of cortical flumazenil binding and blood flow predicting tissue outcome in patients with cerebral ischaemia. Brain. 2001;124:20–9.
60. Guadagno JV, Jones PS, Aigbirhio FI, Wang D, Fryer TD, Day DJ, et al. Selective neuronal loss in rescued penumbra relates to hypoperfusion. Brain. 2008;131:2666–78.
61. Hatazawa J, Satoh T, Shimosegawa E, Okudera T, Inugami A, Ogawa T, et al. Evaluation of cerebral infarction with iodine 123-iomazenil SPECT. J Nucl Med. 1995;36:2154–61.
62. Nakagawara J, Sperling B, Lassen NA. Incomplete brain infarction of reperfused cortex may be quantitated with iomazenil. Stroke. 1997;28:124–32.
63. Dong Y, Fukuyama H, Nabatame H, Yamauchi H, Shibasaki H, Yonekura Y. Assessment of benzodiazepine receptors using iodine-123-labeled iomazenil single-photon emission computed tomography in patients with ischemic cerebrovascular disease. A comparison with PET study. Stroke. 1997; 28:1776–82.
64. Saur D, Buchert R, Knab R, Weiller C, Röther J. Iomazenil-single-photon emission computed tomography reveals selective neuronal loss in magnetic resonance-defined mismatch areas. Stroke. 2006;37:2713–9.
65. Chapman JD, Baer K, Lee J. Characteristics of the metabolism-induced binding of misonidazole to hypoxic mammalian cells. Cancer Res. 1983;43:1523–8.
66. Hoffman JM, Rasey JS, Spence AM, Shaw DW, Krohn KA. Binding of the hypoxia tracer [^{3}H]misonidazole in cerebral ischemia. Stroke. 1987;18:168–76.
67. Mathias CJ, Welch MJ, Kilbourn MR, Jerabek PA, Patrick TB, Raichle ME, et al. Radiolabeled hypoxic cell sensitizers: tracers for assessment of ischemia. Life Sci. 1987;41:199–206.
68. Read SJ, Hirano T, Abbott DF, Sachinidis JI, Tochon-Danguy HJ, Chan JG, et al. Identifying hypoxic tissue after acute ischemic stroke using PET and 18F-fluoromisonidazole. Neurology. 1998;51:1617–21.
69. Read SJ, Hirano T, Abbott DF, Markus R, Sachinidis JI, Tochon-Danguy HJ, et al. The fate of hypoxic tissue on 18F-fluoromisonidazole positron emission tomography after ischemic stroke. Ann Neurol. 2000;48:228–35.
70. Markus R, Reutens DC, Kazui S, Read S, Wright P, Chambers BR, et al. Topography and temporal evolution of hypoxic viable tissue identified by 18F-fluoromisonidazole positron emission tomography in humans after ischemic stroke. Stroke. 2003; 34:2646–52.
71. Spratt NJ, Ackerman U, Tochon-Danguy HJ, Donnan GA, Howells DW. Characterization of fluoromisonidazole binding in stroke. Stroke. 2006;37:1862–7.
72. Bowler JV, Wade JP, Jones BE, Nijran KS, Steiner TJ. Natural history of spontaneous reperfusion of human cerebral infarcts as assessed by ^{99m}Tc HMPAO SPECT. J Neurol Neurosurg Psychiatry. 1998;64:90–7.
73. Oku N, Matsumoto M, Hashikawa K, Moriwaki H, Ishida M, Seike Y, et al. Intra-individual differences between technetium-99m-HMPAO and technetium-99m-ECD in the normal medial temporal lobe. J Nucl Med. 1997;38:1109–11.
74. Asenbaum S, Brücke T, Pirker W, Pietrzyk U, Podreka I. Imaging of cerebral blood flow with technetium-99m-HMPAO and technetium-99m-ECD: a comparison. J Nucl Med. 1998; 39:613–8.
75. Sperling B, Lassen NA. Hyperfixation of HMPAO in subacute ischemic stroke leading to spuriously high estimates of cerebral blood flow by SPECT. Stroke. 1993;24:193–4.
76. Cho I, Hayashida K, Imakita S, Kume N, Fukuchi K. Hemodynamic and metabolic state of hyperfixation with ^{99m}Tc-HMPAO brain SPECT in subacute stroke. Ann Nucl Med. 2000;14:159–63.
77. Colamussi P, Calò G, Sbrenna S, Uccelli L, Bianchi C, Cittanti C, et al. New insights of flow-independent mechanisms of ^{99m}Tc-HMPAO retention in nervous tissue: in vivo study. J Nucl Med. 1999;40:1556–62.
78. Fujibayashi Y, Taniuchi H, Waki A, Yokoyama A, Ishii Y, Yonekura Y. Intracellular metabolism of 99mTc-d, l-HMPAO in vitro: a basic approach for understanding the hyperfixation mechanism in damaged brain. Nucl Med Biol. 1998;25:375–8.
79. Yamada N, Imakita S, Sakuma T. Value of diffusion-weighted imaging and apparent diffusion coefficient in recent cerebral infarctions: a correlative study with contrast-enhanced T1-weighted imaging. AJNR Am J Neuroradiol. 1999;20:193–8.
80. Lassen NA, Sperling B. ^{99m}Tc-bicisate reliably images CBF in chronic brain diseases but fails to show reflow hyperemia in subacute stroke: report of a multicenter trial of 105 cases comparing ^{133}Xe and ^{99m}Tc-bicisate (ECD, neurolite) measured by SPECT on same day. J Cereb Blood Flow Metab. 1994;Suppl 1:S44–8.
81. Tsuchida T, Nishizawa S, Yonekura Y, Sadato N, Iwasaki Y, Fujita T, et al. SPECT images of technetium-99m-ethyl cysteinate dimer in cerebrovascular diseases: comparison with other cerebral perfusion tracers and PET. J Nucl Med. 1994;35:27–31.
82. Tamgac F, Moretti JL, Defer G, Weinmann P, Roussi A, Cesaro P. Non-matched images with ^{123}I-IMP and ^{99m}Tc-bicisate single-photon emission tomography in the demonstration of focal hyperemia during the subacute phase of an ischaemic stroke. Eur J Nucl Med. 1994;21:254–7.
83. Shishido F, Uemura K, Inugami A, Ogawa T, Fujita H, Shimosegawa E, et al. Discrepant ^{99m}Tc-ECD images of CBF in patients with subacute cerebral infarction: a comparison of CBF, $CMRO_2$ and ^{99m}Tc-HMPAO imaging. Ann Nucl Med. 1995;9:161–6.
84. Ogasawara K, Ogawa A, Ezura M, Konno H, Doi M, Kuroda K, et al. Dynamic and static ^{99m}Tc-ECD SPECT imaging of subacute cerebral infarction: comparison with ^{133}Xe SPECT. J Nucl Med. 2001;42:543–7.
85. Walovitch RC, Cheesman EH, Maheu LJ, Hall KM. Studies of retention mechanism of the brain perfusion imaging agent ^{99m}Tc-bicisate (^{99m}Tc-ECD). J Cereb Blood Flow Metab. 1994;Suppl 1:S4–11.
86. Inoue Y, Abe O, Kawakami T, Ozaki T, Inoue M, Yokoyama I, et al. Metabolism of ^{99m}Tc-ethylcysteinate dimer in infarcted brain tissue of rats. J Nucl Med. 2001;42:802–7.
87. Block M, Zecca L, Hong JS. Microglia-mediated neurotoxicity: uncovering the molecular mechanisms. Nat Rev Neurosci. 2007;8:57–69.
88. Hanisch UK, Kettenmann H. Microglia: active sensor and versatile effector cells in the normal and pathologic brain. Nat Neurosci. 2007;10:1387–94.
89. Neumann H, Kotter MR, Franklin RJ. Debris clearance by microglia: an essential link between degeneration and regeneration. Brain. 2009;132:288–95.
90. Benavides J, Cornu P, Dennis T, Dubois A, Hauw JJ, MacKenzie ET, et al. Imaging of human brain lesions with an omega 3 site radioligand. Ann Neurol. 1988;24:708–12.
91. Gerhard A, Neumaier B, Elitok E, Glatting G, Ries V, Tomczak R, et al. In vivo imaging of activated microglia using [^{11}C]PK11195 and positron emission tomography in patients after ischemic stroke. Neuroreport. 2000;11:2957–60.

92. Gerhard A, Schwarz J, Myers R, Wise R, Banati RB. Evolution of microglial activation in patients after ischemic stroke: a [^{11}C](R)-PK11195 PET study. Neuroimage. 2005;24:591–5.
93. Price CJ, Wang D, Menon DK, Guadagno JV, Cleij M, Fryer T, et al. Intrinsic activated microglia map to the peri-infarct zone in the subacute phase of ischemic stroke. Stroke. 2006;37:1749–53.
94. Rojas S, Martín A, Arranz MJ, Pareto D, Purroy J, Verdaguer E, et al. Imaging brain inflammation with [^{11}C]PK11195 by PET and induction of the peripheral-type benzodiazepine receptor after transient focal ischemia in rats. J Cereb Blood Flow Metab. 2007;27:1975–86.
95. Schroeter M, Dennin MA, Walberer M, Backes H, Neumaier B, Fink GR, et al. Neuroinflammation extends brain tissue at risk to vital peri-infarct tissue: a double tracer [^{11}C]PK11195- and [^{18}F]FDG-PET study. J Cereb Blood Flow Metab. 2009;29: 1216–25.
96. Radlinska BA, Ghinani SA, Lyon P, Jolly D, Soucy JP, Minuk J, et al. Multimodal microglia imaging of fiber tracts in acute subcortical stroke. Ann Neurol. 2009;66:825–32.
97. Yuan J. Neuroprotective strategies targeting apoptotic and necrotic cell death for stroke. Apoptosis. 2009;14:469–77.
98. Broughton BR, Reutens DC, Soby CG. Apoptotoic mechanisms after cerebral ischemia. Stroke. 2009;40:e331–9.
99. Seigneuret M, Devaux PF. ATP-dependent asymmetric distribution of spin-labeled phospholipids in the erythrocyte membrane: relation to shape changes. Proc Natl Acad Sci USA. 1984;81:3751–5.
100. Diaz C, Schroit AJ. Role of translocases in the generation of phosphatidylserine asymmetry. J Membr Biol. 1996;151:1–9.
101. Fadok VA, Voelker DR, Campbell PA, Cohen JJ, Bratton DL, Henson PM. Exposure of phosphatidylserine on the surface of apoptotic lymphocytes triggers specific recognition and removal by macrophages. J Immunol. 1992;148:2207–16.
102. Andree HA, Reutelingsperger CP, Hauptmann R, Hemker HC, Hermens WT, Willems GM. Binding of vascular anticoagulant alpha (VAC alpha) to planar phospholipid bilayers. J Biol Chem. 1990;265:4923–8.
103. Martin SJ, Reutelingsperger CP, McGahon AJ, Rader JA, van Schie RC, LaFace DM, et al. Early redistribution of plasma membrane phosphatidylserine is a general feature of apoptosis regardless of the initiating stimulus: inhibition by overexpression of Bcl-2 and Abl. J Exp Med. 1995;182:1545–56.
104. Blankenberg FG, Kalinyak J, Liu L, Koike M, Cheng D, Goris ML, et al. ^{99m}Tc-HYNIC-annexin V SPECT imaging of acute stroke and its response to neuroprotective therapy with anti-Fas ligand antibody. Eur J Nucl Med Mol Imaging. 2006;33:566–74.
105. Lorberboym M, Blankenberg FG, Sadeh M, Lampl Y. In vivo imaging of apoptosis in patients with acute stroke: correlation with blood-brain barrier permeability. Brain Res. 2006;1103: 13–9.

Ann Nucl Med (2011) 25:189–196
DOI 10.1007/s12149-010-0438-y

ORIGINAL ARTICLE

Omission of [^{15}O]CO scan for PET $CMRO_2$ examination using ^{15}O-labelled compounds

Yasuhiro Sasakawa · Nobuyuki Kudomi · Yuka Yamamoto · Toshihide Monden · Nobuyuki Kawai · Yoshihiro Nishiyama

Received: 15 September 2010 / Accepted: 12 October 2010 / Published online: 16 November 2010

Abstract
Objective CBF, OEF and $CMRO_2$ provide us important clinical indices and are used for assessing ischemic degree in cerebrovascular disorders. These quantitative images can be measured by PET using ^{15}O-labelled tracers such as $C^{15}O$, $C^{15}O_2$ and $^{15}O_2$. To reduce the time of scan, one possibility is to omit the use of CBV data. The present study investigated the influence of fixing the CBV to OEF and $CMRO_2$ values on subjects with and without cerebrovascular disorders.
Methods The study consisted of three groups, namely, GROUP-0 ($n = 10$), GROUP-1 ($n = 9$), and GROUP-2 ($n = 10$), corresponding to—without significant disorder, with elevated CBV, and with reduced CBF and elevated OEF, respectively. All subjects received PET examination and using the PET data OEF and $CMRO_2$ images were computed by fixing CBV and with CBV data. The computed OEF and $CMRO_2$ values were compared between the methods.
Results The OEF and $CMRO_2$ values obtained by fixing the CBV were around 10% underestimation against that with CBV data. The regression analysis showed that these values were comparable ($r = 0.93$–0.98, $P < 0.001$). The simulation showed that fixing of the CBV would not derive significant error in either OEF or $CMRO_2$ values, when changed from 0 to 0.08 ml/g.
Conclusion This study shows the feasibility of fixing the CBV value for computing OEF and $CMRO_2$ values in the PET examination, suggesting the CO scan could be eliminated.

Keywords Positron emission tomography · CBF · $CMRO_2$ · CBV · ^{15}O-labelled compounds

Y. Sasakawa (✉) · T. Monden
Department of Clinical Radiology, Kagawa University Hospital, 1750-1 Ikenobe, Miki-cho, Kita-gun, Kagawa 761-0793, Japan
e-mail: sasakawa@med.kagawa-u.ac.jp

N. Kudomi
Department of Medical Physics, Faculty of Medicine, Kagawa University, Kagawa, Japan

Y. Yamamoto · Y. Nishiyama
Department of Radiology, Faculty of Medicine, Kagawa University, Kagawa, Japan

N. Kawai
Department of Neurological Surgery, Faculty of Medicine, Kagawa University, Kagawa, Japan

Introduction

Cerebral blood flow (CBF), oxygen extraction fraction (OEF), and cerebral metabolic rate of oxygen ($CMRO_2$) provide us important clinical indices that can be used for assessing ischemic degree in chronic and acute cerebral arterial occlusive diseases. These functional images can be quantitatively measured by positron emission tomography (PET) using ^{15}O-labelled compounds. Several quantitative approaches to obtain CBF and $CMRO_2$ images have been developed and applied in clinical assessment. The computational formulae to compute these parametric images are based on a single-tissue compartment model for oxygen and water kinetics [1–4], and generally require data set of $C^{15}O$ scan for CBV, $C^{15}O_2$ or $H_2{}^{15}O$ scan for CBF and $^{15}O_2$ together with CBF and CBV for OEF and $CMRO_2$.

In the steady-state method [4–9], the parametric images are estimated from the data set which is acquired while in

the steady state reached during the continuous inhalation of $^{15}O_2$ and $C^{15}O_2$ as well as bolus inhalation of $C^{15}O$, requiring waiting time to reach equilibrium. The autoradiographic method, which applies separate bolus administration of three traces of CO, CO_2 (or $H_2{}^{15}O$) and O_2 (three-step ARG), has also been employed [3, 10, 11]. Recently, Kudomi et al. [12, 13] developed a dual tracer autoradiographic (DARG) method to shorten the PET examination period. This method applies sequential administration of dual tracers of $^{15}O_2$ and $C^{15}O_2$ ($^{15}O_2$–$C^{15}O_2$ scan) during a single PET scan, and computed CBF and $CMRO_2$ by the autoradiographic manner.

In previous studies, it is suggested that the degree of error propagated from error on CBV value is small in OEF and $CMRO_2$ values from normal and simulation data [6, 12]. These findings suggest a possibility of neglecting or fixing the CBV value in the computation the OEF and $CMRO_2$ without significant bias. However, it has not been systematically studied how the OEF and $CMRO_2$ computed in that fashion are affected by the fluctuation and/or change of CBV values on diseased brain region as well as normal region.

In this study, we investigated the influence of fixing of CBV to the OEF and $CMRO_2$ values using our CBF–$CMRO_2$ PET examination data on subjects with and without cerebrovascular disorders. Also, we investigated the size of error when these OEF and $CMRO_2$ are computed by fixing the CBV value in a simulation study.

Materials and methods

Subjects

Subjects were retrospectively selected from a clinical data base in our hospital. All subjects received PET examination due to suspected cerebrovascular disorders for a period of January to December in 2008. According to Powers' classification of chronic hemodynamics compromised with occlusive cerebrovascular disease [14], hemodynamic impairment can be categorized into two stages. Stage I is defined as an increase in CBV in the hemisphere distal to the occlusive lesion, with normal CBF, OEF, and $CMRO_2$. Stage II is characterized by reduced CBF and increased OEF with normal $CMRO_2$. These stages were originally defined using steady-state method [4–9], and cannot be directly applied to the present subjects because of different PET measurement procedures. We separate the subjects to following three groups: GROUP-0 consisted of subjects who are diagnosed without significant disorder from PET parametric images, namely, there were no apparent difference in arterial territories between hemispheres in CBV, CBF, OEF and $CMRO_2$ images and these values in 12.5 mm circular ROI ranged 0.02–0.05 ml/g, 0.4–0.6 ml/min/g, 0.35–0.50, and 0.020–0.045 ml/min/g, respectively ($n = 10$, 6 males and 4 females, weight = 56.8 ± 12.0 kg, age = 60.6 ± 18.7 years). GROUP-1 consisted of patients diagnosed with chronic stenosis or occlusion with elevated CBV, namely, arterial territory region(s) with >30% difference was included in ipsi-hemisphere against contralateral-hemisphere in CBV image. And no apparent change in arterial territories between hemispheres in CBF, OEF and $CMRO_2$, namely, these values ranged same as the GROUP-0 condition ($n = 9$, 7 males and 2 females, weight = 60.0 ± 14.1 kg, age = 65.7 ± 14.7 years). GROUP-2 consisted of patients diagnosed with chronic stenosis or occlusion with reduced CBF, elevated OEF, namely, arterial territory region(s) with >20% reduction and >10% elevation was included in ipsi-hemisphere against contralateral-hemisphere in CBF and OEF images, respectively ($n = 10$, 9 males and 1 female, weight = 62.4 ± 11.1 kg, age = 65.6 ± 12.4 years). All patients gave written consent to participate in the study, which was approved by our University Ethical Committee.

PET measurement protocol

PET acquisition was carried out in 2D mode using the Siemens ECAT HR^+ scanner (Siemens-CTI, Knoxville, USA), which provided 63 tomographic slice images for an axial field-of-view of approximately 150 mm. After 300 s transmission scan, a PET scan was started at 4 min after $C^{15}O$ (2 GBq/min) inhalation for 1 min. Blood samples (~1 mL) were taken from the right radial artery at 300, 360 and 420 s after the start time of the inhalation. Radioactivity concentration in blood was measured with a well counter ARC400 (Aloka, Mitaka, Tokyo, Japan). The detectors had been cross-calibrated to the PET scanner. After 5 min of the $C^{15}O$ scan, a PET scan and $C^{15}O_2$ (1.5 GBq/min) inhalation were started simultaneously. The inhalation was continued for 2 min. The scan protocol consisted of 23 frames with total of 600 s (1 × 30 s, 10 × 15 s, 10 × 30 s and 2 × 60 s). During the $C^{15}O_2$ scan, blood was manually sampled (~1 mL) through a catheter inserted in the right radial artery at 30, 45, 60 75, 90, 105, 120, 135, 150, 165, 180, 210, 240, 270, 300, 360, 420, 480, 540 and 600 s from the PET start time. Radioactivity concentration in blood was measured with the well counter. Then, each subject continuously inhaled 500 MBq/min $^{15}O_2$ for 12 min. After 7 min of the start time of the inhalation, the scan was started and continued for 5 min. During the scan, blood (~1 mL) was manually sampled from the right radial artery at 480, 600 and 720 s from the start time of the inhalation. The radioactivity concentration was measured using the well counter.

Data processing

Dynamic sinogram data were corrected for dead time in each frame in addition to detector normalization. Tomographic images were reconstructed from corrected sinogram data by the filtered back-projection method using a Hann filter. Attenuation correction was applied with transmission data. A reconstructed image consisted 128 × 128 × 63 matrix size with a pixel size of 1.7 mm × 1.7 mm and 2.4 mm with 23 frames.

Measured arterial blood time activity curves (TAC) obtained in $C^{15}O_2$ examination were calibrated to the PET scanner and corrected for dispersion ($\tau = 5$) [15] and delay [16]. The corrected blood TAC was used as the input function.

Computation of CBV, CBF, OEF and $CMRO_2$

CBV

CBV (V_B) was calculated from the $C^{15}O$ scan data and blood activity sampled during the scan as [3]:

$$V_B = \frac{C_{CO}}{R_{Hct} \times \rho_{brain} \times A_{CO} \times \rho_{blood}} \quad (1)$$

where $C_{CO}(t)$ (Bq/ml) is radioactivity concentration in a voxel of PET image, and ρ_{brain} and ρ_{blood} indicate the brain tissue (=1.06 g/ml) and blood (=1.04 g/ml) specific gravity, respectively. A_{CO} (Bq/ml) is the radioactivity concentration for $C^{15}O$ in the arterial blood and R_{Hct} is the small-to-large vessel hematocrit ratio.

CBF

In the present computation, we have applied a basis function method (BFM) to obtain the CBF image. The method was introduced by Koeppe et al. [17] to compute CBF as well as washout images using linear least squares together with a discretised range of basis functions incorporating the nonlinearity and covering the expected physiological range. The kinetic model for $H_2{}^{15}O$ was based on the single-tissue compartment model as:

$$Ci(t) = (1 - V_A) \times K_1 \times A_w(t) \otimes e^{-k_2 t} + V_A \times A_w(t) \quad (2)$$

where K_1 (=*f*:CBF) (ml/min/g) and k_2 (ml/g) are uptake and clearance rate constants, respectively, V_A (ml/g) is activity concentration in arterial vascular space, $Ci(t)$ (Bq/ml) is radioactivity concentration in a voxel of PET image, $A_w(t)$ (Bq/mL) is the arterial input function, $\otimes$ indicates the convolution integral. This method allows dealing with nonlinear term by choosing a discrete spectrum of parameter values for k_2. The corresponding basis function formed as;

$$F(f,t) = A_w(t) \otimes e^{-k_2 t} \quad (3)$$

Then, Eq. 2 can be transformed for each basis function into a linear equation in $\Theta(=(1 - V_A)K_1)$ and $\Psi(=V_A)$ as:

$$Ci(t) = \Theta \times F + \Psi \times A_w. \quad (4)$$

Hence for fixed values of k_2, the remaining two parameters Θ and Ψ can be estimated using standard linear least squares. The k_2 for which the residual sum of square is minimized is determined by a direct search and associated parameter values for this solution (K_1, k_2, V_A) are obtained. For the physiologically reasonable range of k_2, i.e., $0 < k_2 < 2.0$ ml/min/g, 200 discrete values for k_2 were found to be sufficient and CBF as well as k_2 and V_A were obtained.

OEF and $CMRO_2$

OEF (E) and $CMRO_2$ ($K_1^O[O_2]$, where $K_1^O = fE$ and $[O_2]$ is the measured arterial oxygen content [3]) were calculated from the $^{15}O_2$ scan data (C_i^O) and blood activity sampled during the scan. After continuously administrating $^{15}O_2$, the radioactivity distribution of PET count: $C_t(t)$ (Bq/ml), reaches a steady state, and $C_t(t)$ can be expressed as (Eq. 7 in [6]):

$$C_t = \frac{f}{f/V_A + \lambda}\left(\frac{fA'_W/V_A}{f/V_d + \lambda} + \frac{fEA_O/V_A}{f/V_d + \lambda} + \frac{A_O(1-E)F/V_A}{f/V_V + \lambda} + A_O + A'_W\right) \quad (5)$$

where, λ (=0.00567 s^{-1}) is the decay constant of ^{15}O, and V_d is the volume of distribution for extracted water, A_O, and A_W' are the radioactivity concentration of $^{15}O_2$ and recirculating $H_2{}^{15}O$ content in the arterial blood, respectively. V_A and V_V are the arterial and venous volume, thus the blood volume can be expressed as: $V_B = V_A + V_V$.

For practical computation, a first order approximation would neglect the arterial volume and consider all blood volume signals to be at venous concentration [6] as:

$$V_A = 0, V_V = V_B, V_d = V \quad (6)$$

where V is a unit volume for cerebral tissue and blood, i.e., $V = 1$ ml/ml. Then, the OEF and $CMRO_2$ images were computed using the reconstructed oxygen image as well CBF, CBV images (VBM), and radioactivity concentration of $^{15}O_2$ (A_O) and $H_2{}^{15}O$ (A_W) content in the arterial blood. The A_O and A_W contents were calculated from radioactivity concentration of total blood (A_T) by assuming fixing generation ratio as: $A_O = 0.824A_T$ and $A_W = 0.176A_T$ [18–20], respectively. Also, the OEF and $CMRO_2$ images were computed by fixing the value of CBV as a mean of multiple center study as: $V_B = 0.036$ ml/g (VBA) [21], and with fixing value as $V_B = 0$, i.e., ignoring the contribution of radioactivity from blood vessels (VB0).

Data analysis

Circular region of interests (ROI) were placed for all subjects on CBF images each in frontal, in temporal, in parietal, in occipital and in cerebellum cortical regions in each hemisphere, respectively, i.e., 30 ROIs were placed in total. The size of ROI was 12.1 mm in diameter. The CBV, CBF, OEF and $CMRO_2$ values were extracted for all ROIs from the obtained images, and mean and SD were computed. Then, the OEF and $CMRO_2$ values were compared by the Student's t test between the methods, i.e., between VBM and VBA, and between VBM and VB0, respectively, and $P < 0.05$ was considered statistically significant. Regression analysis was also performed.

Error analyses in simulation

Error propagation from fixing of CBV values in OEF and $CMRO_2$ values was analysed to reveal the degree of error as well as that of the difference between scan procedures, i.e., difference between the present and the three-step ARG methods [3, 10]. A typical arterial input function obtained from a PET study was used in the present simulation as the true input function. Applying this input function, water and oxygen tissue TACs were created assuming values of normal brain tissue condition ($f = 0.5$ ml/min/g [22], $E = 0.4$ [22]), assumed stage II [14] condition ($f = 0.3$ ml/min/g, $E = 0.6$) and lower $CMRO_2$ condition ($f = 0.25$ ml/min/g and $E = 0.4$, where $CMRO_2$ can be calculated as $fE[O_2]$, thus half the normal condition).

V_B value was varied from 0.0 to 0.08 ml/g [14] and tissue TACs were generated to simulate the size of error. Then, OEF and $CMRO_2$ were calculated using the created tissue TACs assuming $V_B = 0.04$ ml/g [21], i.e., VBA method in this study. Error in OEF and $CMRO_2$ values due to fixing V_B was presented as percent difference of OEF and $CMRO_2$ as a function of V_B.

Results

Experiments

The mean and SD value of CBV for GROUP-0, 1 and 2 were summarized in Table 1. The differences of OEF and $CMRO_2$ values were less than 5% between VBM and VBA, however, they were 9.7% between VBM and VB0. No significant difference was found between VBM and VBA both in OEF and $CMRO_2$, however, the differences were significant between VBM and VB0 both in OEF and $CMRO_2$. The relationships of the regional ROI values of OEF and $CMRO_2$ between VBM and VBA are shown in Fig. 1.

For GROUP-1, the differences of OEF and $CMRO_2$ values were less than 5% between VBM and VBA for both contralateral and ipsi-hemispheres, however, they were 10–13% between VBM and VB0. No significant difference was found between VBM and VBA both in OEF and $CMRO_2$, and both in ipsi- and contralateral hemispheres.

For GROUP-2, the mean of CBV in disease territory was 0.035 ml/g ranging from 0.021 to 0.056 ml/g, 0.33 ml/min/g ranged from 0.29 to 0.36 ml/min/g in CBF, 0.58 from 0.53 to 0.65 in OEF, and 0.033 ml/min/g from 0.029 to 0.038 ml/min/g in $CMRO_2$, respectively. The differences of OEF and $CMRO_2$ values were less than 5% between VBM and VBA both for contralateral and ipsi-hemispheres, however, they were 8–10% between VBM and VB0. No significant difference was found between VBM and VBA both in OEF and $CMRO_2$, and both in ipsi- and contralateral hemispheres.

Table 1 The mean values and SD of normal and disease hemispheres for GROUP-0, GROUP-1 and GROUP-2

	CBV (ml/g)	CBF (ml/min/g)	OEF			$CMRO_2$ (ml/min/g)		
			VBM	VBA	VB0	VBM	VBA	VB0
GROUP-0	0.032 ± 0.012	0.50 ± 0.09	0.43 ± 0.09	0.42 ± 0.09	0.47 ± 0.08[a]	0.034 ± 0.008	0.033 ± 0.008	0.037 ± 0.008[a]
GROUP-1								
Contralateral	0.036 ± 0.018	0.51 ± 0.11	0.45 ± 0.09	0.45 ± 0.09	0.49 ± 0.08[a]	0.035 ± 0.009	0.035 ± 0.009	0.039 ± 0.009[a]
Disease	0.041 ± 0.019	0.50 ± 0.10	0.44 ± 0.08	0.45 ± 0.09	0.50 ± 0.08[a]	0.035 ± 0.009	0.035 ± 0.009	0.039 ± 0.009[a]
GROUP-2								
Contralateral	0.032 ± 0.012	0.45 ± 0.13	0.47 ± 0.09	0.46 ± 0.09	0.51 ± 0.09[a]	0.035 ± 0.007	0.034 ± 0.007	0.038 ± 0.008[a]
Disease	0.036 ± 0.020	0.42 ± 0.13	0.48 ± 0.09	0.48 ± 0.09	0.53 ± 0.09[a]	0.034 ± 0.010	0.034 ± 0.010	0.037 ± 0.011[a]

VBM the OEF and $CMRO_2$ images were computed using the scanned CBV image, *VBA* images were computed fixing the CBV value as 0.036 ml/g, *VB0* these images were computed fixing the CBV value as 0, *GROUP-0* subjects without significant disorder, *GROUP-1* subjects with elevated CBV, *GROUP-2* subjects with reduced CBF and elevated OEF

[a] Significantly different

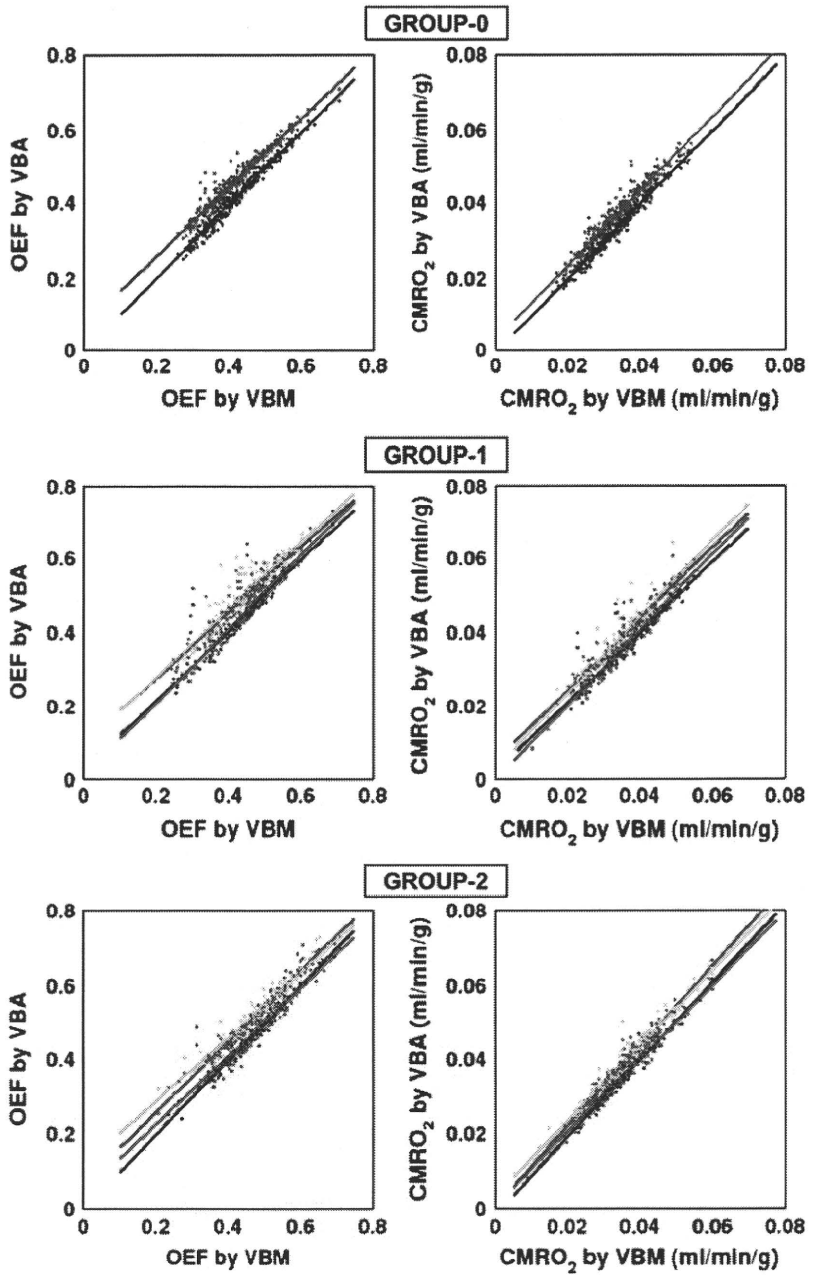

Fig. 1 Relationships of the regional ROI values for GROUP-0, GROUP-1 and GROUP-2 subjects between VBA and VBM, and between VBM and VB0, respectively. The regression lines are shown in each figure, where *black plots and lines* show relation between VBM and VBA and those of *blue and green* show between VBM and VB0. *Black and blue plots and lines* show relation for contralateral and *red and green* show ipsi-lateral hemispheres, respectively. The regression lines (E and M indicate OEF and $CMRO_2$, respectively), GROUP-0: $E_{VBA} = 0.99\ E_{VBM} + 0.00$ ($r = 0.98$, $P < 0.001$), $M_{VBA} = 1.00\ M_{VBM} - 0.001$ ml/min/g ($r = 0.98$, $P < 0.001$) between VBM and VBA; $E_{VBA} = 0.93\ E_{VBM} + 0.07$ ($r = 0.98$, $P < 0.001$), $M_{VBA} = 1.01\ M_{VBM} - 0.002$ ml/min/g ($r = 0.97$, $P < 0.001$) between VBM and VB0. GROUP-1 contralateral: $E_{VBA} = 0.95\ E_{VBM} - 0.02$ ($r = 0.95$, $P < 0.001$), $M_{VBA} = 0.95\ M_{VBM} + 0.002$ ml/min/g ($r = 0.97$, $P < 0.001$) between VBM and VBA, and $E_{VBA} = 0.89\ E_{VBM} - 0.10$ ($r = 0.94$, $P < 0.001$), $M_{VBA} = 0.97\ M_{VBM} + 0.005$ ml/min/g ($r = 0.97$, $P < 0.001$) between VBM and VB0, ipsi-lateral: $E_{VBA} = 1.00\ E_{VBM} - 0.01$ ($r = 0.96$, $P < 0.001$), $M_{VBA} = 1.03\ M_{VBM} + 0.001$ ml/min/g ($r = 0.96$, $P < 0.001$) between VBM and VBA and $E_{VBA} = 0.92\ E_{VBM} - 0.09$ ($r = 0.93$, $P < 0.001$), $M_{VBA} = 1.04\ M_{VBM} + 0.003$ ml/min/g ($r = 0.96$, $P < 0.001$) between VBM and VB0. GROUP-2, contralateral: $E_{VBA} = 1.00\ E_{VBM} - 0.01$ ($r = 0.98$, $P < 0.001$), $M_{VBA} = 1.04\ M_{VBM} - 0.002$ ml/min/g ($r = 0.99$, $P < 0.001$) between VBM and VBA and $E_{VBA} = 0.96\ E_{VBM} - 0.06$ ($r = 0.98$, $P < 0.001$), $M_{VBA} = 1.08\ M_{VBM} - 0.000$ ml/min/g ($r = 0.98$, $P < 0.001$) between VBM and VB0; ipsi-lateral: $E_{VBA} = 0.92\ E_{VBM} - 0.04$ ($r = 0.94$, $P < 0.001$), $M_{VBA} = 0.99\ M_{VBM} - 0.001$ ml/min/g ($r = 0.97$, $P < 0.001$) between VBM and VBA; $E_{VBA} = 0.86\ E_{VBM} - 0.11$ ($r = 0.94$, $P < 0.001$), $M_{VBA} = 1.02\ M_{VBM} - 0.003$ ml/min/g ($r = 0.97$, $P < 0.001$) between VBM and VB0